

Magnetic hardness of hexagonal and orthorhombic Fe_3C , Co_3C , $(\text{Fe-Co})_3\text{C}$, and their alloys with boron, nitrogen, and transition metals: A first-principles study

Justyn Snarski-Adamski, Mirosław Werwiński,* and Justyna Rychły-Gruszecka
*Institute of Molecular Physics, Polish Academy of Sciences,
 M. Smoluchowskiego 17, 60-179 Poznań, Poland*

(Dated: October 8, 2024)

Restrictions on the availability of rare earth metals create a strong demand for new rare-earth-free hard magnetic materials. In this study, we considered a large set of materials that are closely related to orthorhombic Fe_3C (cementite) with the aim of characterizing trends in their intrinsic magnetic properties, highlighting the relation between magnetic properties and the chemical composition, and identifying alloys that are optimal for applications. A comprehensive analysis was conducted on the full concentration ranges of hexagonal (ϵ) and orthorhombic (θ) phases of $(\text{Fe-Co})_3\text{C}$, $(\text{Fe-Co})_3(\text{B-C})$, $(\text{Fe-Co})_3(\text{C-N})$, and their alloys with $3d$, $4d$ and $5d$ transition metals. The calculations were performed using the density functional theory implemented in the full-potential local-orbital code (FPLO). Calculated properties included formation energies, Curie temperatures, magnetic moments, magnetocrystalline anisotropy energies (MAE), and magnetic hardnesses. The considered compositions exhibit a range of magnetic properties, including soft, semi-hard, and hard magnetic. The materials most promising for hard-magnetic applications are selected Co-rich orthorhombic and hexagonal $(\text{Fe,Co})_3\text{C}$ alloys. The calculation results do not indicate that substituting with transition metals increases the potential of the alloys for permanent magnet applications. A significant drawback of alloying orthorhombic $\theta\text{-Fe}_3\text{C}$ (cementite) with transition metals is the notable decline in the Curie temperature. Among the positive outcomes, we found that a considerable proportion of the orthorhombic $\text{Co}_3(\text{B-C-N})$ alloys are magnetically hard, of which boron substitution raises the Curie temperature and improves stability. By mapping the dependence of MAE on the concentration of elements covering both the $3d$ (from Fe to Co) and $2p$ (from B, through C, to N) positions, we have demonstrated for the first time the near isoelectronic nature of MAE. The latter observation may be particularly useful in designing compositions of new magnetically hard materials.

I. INTRODUCTION

Permanent magnets are an essential component of modern technology [1–3]. Demand for neodymium magnets reached 119.2 thousand tons in 2020 and is growing [4]. However, there are potential risks associated with the use of neodymium magnets, such as limited availability of neodymium and strong fluctuations of its price. The significant increase in price of rare-earth metals that took place around 2011 is referred to as the *2011 rare-earth crisis* [5]. A similar economic situation was repeated in 2022. For the above reasons, it is important to identify new materials for permanent magnet applications that require minimal or no rare earth elements [6–11].

In this work, we will focus on Fe_3C -based alloys intensively studied for more than a decade as promising materials for permanent magnets [12–19].

In this study, we present a first-principles analysis of the hexagonal iron carbide $\epsilon\text{-Fe}_3\text{C}$ (referred to hereafter as hexa- Fe_3C), the orthorhombic cementite $\theta\text{-Fe}_3\text{C}$ (referred to hereafter as ortho- Fe_3C), and the corresponding Co_3C phases (hexa- Co_3C and ortho- Co_3C). Moreover, we calculate a series of Fe_3C and Co_3C alloys with transition metal elements $3d$, $4d$, and $5d$ and also consider the $(\text{Fe,Co})_3\text{C}$ and $(\text{Fe,Co})_3(\text{B,C,N})$ alloys.

When discussing Fe_3C and Co_3C alloys for use as permanent magnets, we will focus primarily on two intrinsic properties of the materials, magnetocrystalline anisotropy energy (MAE) and Curie temperature (T_C). The experimental value of the uniaxial magnetocrystalline anisotropy constant of ortho- Fe_3C is a moderate 0.405 MJ m^{-3} at 5 K [20]. Whereas, the measured Curie temperature for ortho- Fe_3C is 481 K [21]. The state of the knowledge on the properties of ortho- Fe_3C (cementite) is summarized by Bhadeshia [22]. The ortho- Co_3C shows an experimental MAE of $0.74 \pm 0.1 \text{ MJ m}^{-3}$ and Curie temperature of 650 K [23]. Additionally, Co_3C carbide nanocrystals have been confirmed to possess hard magnetic properties [12]. Enhanced magnetocrystalline anisotropy has been also observed in Co-C nanowires, Co-C nanoparticles, and polyphase Fe-Co-C polycrystalline samples [15, 23, 24]. The melt-spun Fe_2CoC alloys show elevated magnetocrystalline anisotropy constant (K_1) of 0.91 MJ m^{-3} and magnetic moment of $1.23 \mu_B \text{ atom}^{-1}$ (at 10 K) [17]. In contrast, an exceptionally high K_1 of 4.6 MJ m^{-3} has been measured for Fe_2CoC nanoparticles [15].

Fe_3C compositions with transition metals were also experimentally studied, among others: Ti, V, Cr, Mn, Ni, and Mo [25–28]. It was determined what effect the selected substitutions have on the lattice parameters [25] and Curie temperature [26]. It was also found that Cr, Mn, V, and Mo stabilize the alloy, while Ti and Ni destabilize it [27].

Another type of modification of Fe_3C that significantly affects properties is alloying with boron or nitrogen in

* Corresponding author: Mirosław Werwiński
 Email address: werwinski@ifmpan.poznan.pl

place of carbon [21, 29]. For example, it has been shown experimentally that going from Fe_3C to Fe_3B the Curie temperature increases linearly from 481 K to 824 K [21].

Recently, based on first-principles calculations combined with a structure prediction algorithm, positive formation energies (indicating instability) have been determined for the well-known iron carbides and for a large set of newly determined iron carbides [43]. Direct studies on Fe_3C were also carried out using first-principle calculations [30, 44]. The average spin magnetic moments have been estimated as 1.50 and 1.40 μ_B atom $^{-1}$ for the hexa- and ortho- Fe_3C phases, respectively [44]. For details, like spin magnetic moment on Fe and C sites, please check the Table I.

To improve stability and determine magnetic properties, first-principles calculations have been repeatedly used to model cementite alloys with Cr [32, 34, 40, 45–47], Mn [34, 46], Co [17, 48, 49], and Ni [48, 49]. Whereas, the broader context is complemented by calculations of wide ranges of transition metal substitutions in ortho- Fe_3C [33, 50, 51].

First-principles calculations were also made for orthorhombic cementite-type and hexagonal ϵ phases of Fe_3B and Fe_3N compounds [30, 52]. The full range of alloy concentrations of ortho- $\text{Fe}_3(\text{C}_{1-y}\text{B}_y)$ was modeled by the supercell method [53]. Furthermore, Al, Si, P, and S were considered at the C site in the cementite [50]. In addition, in our previous work we already considered $\text{Fe}_{0.7}\text{Co}_{0.3}$ thin films with B, C, and N atoms in interstitial positions [54].

This study, covers the wide ranges of alloying with transition metals, boron, nitrogen, and, going beyond previous reports, focuses on determination of magnetic hardnesses and Curie temperatures – two parameters especially important for permanent magnet applications.

II. CALCULATIONS DETAILS

The calculations were done using density functional theory (DFT) implemented in the full-potential local-orbital code (FPLO18.00-52) [57]. The FPLO includes relativistic effects in the full four-component formalism [58]. Unless otherwise specified, the generalized gradient approximation (GGA) proposed by Perdew, Burke, and Ernzerhof (PBE) [59] was used. For Brillouin zone integration, a tetrahedron method was used, with a mesh of k -points set to $40 \times 40 \times 40$. All calculations were fully converged with a density criterion of 10^{-7} .

The initial structural data for hexagonal ϵ - Fe_3C and orthorhombic θ - Fe_3C phase were taken from experiment [55, 56], see Table II and Fig. 1. Hexa- and ortho- Co_3C structures were prepared using initial data for Fe_3C phases. The volumes of all considered structures were optimized. For hexagonal structures, the ratio of c/a lattice parameters was optimized as well. Wyckoff's positions were optimized in each system using forces with convergence criterion set to 10^{-3} eV \AA^{-1} within a scalar-relativistic approach and with spin polarization, see Ta-

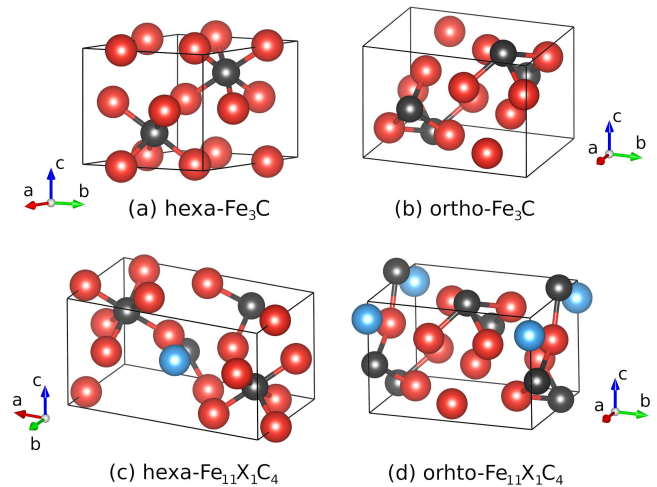


FIG. 1. Crystal structures of (a) hexa- Fe_3C and (b) ortho- Fe_3C , together with corresponding structures of (c,d) hexa- and ortho- $\text{Fe}_{11}\text{X}_1\text{C}_4$ alloys substituted with transition metal element X. Iron, carbon, and transition metal atoms are represented by red, black, and blue spheres, respectively.

ble II. The crystal structures were visualized with the VESTA program [60].

To determine the magnetocrystalline anisotropy energy (MAE), following the completion of self-consistent scalar-relativistic calculations, single iterations of fully relativistic calculations were conducted for orthogonal directions of the magnetization. To analyze the effect of the form of the exchange-correlation potential on the magnetic moment and MAE, the von Barth and Hedin (vBH) [61], Perdew and Zunger (PZ) [62], Perdew and Wang (PW92) [63], and exchange-only (x-only) forms of the local spin density approximation (LSDA) were used in addition to the Perdew-Burke-Ernzerhof (PBE) [59] potential used throughout the paper. In order to ascertain the dependency of the MAE on the magnetic moment, a fully relativistic approach was employed, utilizing of the fixed-spin-moment (FSM) method.

The virtual crystal approximation (VCA) was used to model the $(\text{Fe},\text{Co})_3\text{C}$ alloys and alloying with B and N at the C position. For the pseudobinary $(\text{Fe},\text{Co})_3(\text{B},\text{C},\text{N})$ alloys, a total of 231 compositions for both hexagonal and orthorhombic phase was prepared and evaluated. In order to calculate structures with different percentages of Fe and Co, the lattice parameters and Wyckoff positions were averaged proportionally according to the Fe and Co content of the structure.

To consider $\frac{1}{12}$ substitution of the Fe atoms with $3d$, $4d$, and $5d$ elements, the symmetry of both unit cells was reduced, see Fig. 1. In the case of hexa- $\text{Fe}_{11}\text{X}_1\text{C}_4$ alloys, the space group was reduced to $P121$, while for ortho- $(\text{Fe}/\text{Co})_{11}\text{X}_1\text{C}_4$ alloys, the space group was reduced to $P1m1$. For supercells, the mesh of k -points was set to $25 \times 25 \times 25$, while the charge density criterion was 10^{-7} . In all supercells, the lattice parameters were taken as they were in the initial optimized compounds, whereas

TABLE I. Total spin magnetic moments [total m_s (μ_B f.u. $^{-1}$)] calculated for hexa-Fe₃C, hexa-Co₃C, ortho-Fe₃C and ortho-Co₃C, together with contributions from Fe, Co, and C sites [$m_s(\text{Fe/Co/C})$ (μ_B atom $^{-1}$)]. For orthorhombic phases, magnetic moments on general and special positions of Fe and Co are presented. Our results obtained using the FPLO18 code with PBE exchange-correlation potential are compared with previous calculation outcomes from literature.

hexa-Fe ₃ C				
	$m_s(\text{Fe})$	$m_s(\text{C})$	total m_s	
FPLO, GGA(PBE) [this work]	2.12	-0.30	6.04	
VASP, PAW, GGA [17]	-	-	5.92	
CASTEP, PBE-GGA [30, 31]	(2.04 - 2.23)	(-0.26 - -0.24)	(5.90 - 6.42)	
hexa-Co ₃ C				
	$m_s(\text{Co})$	$m_s(\text{C})$	total m_s	
FPLO, GGA(PBE) [this work]	1.03	-0.12	2.95	
VASP, PAW, GGA [17]	-	-	2.76	
ortho-Fe ₃ C				
	$m_s(\text{Fe}^g)$	$m_s(\text{Fe}^s)$	$m_s(\text{C})$	total m_s
FPLO, GGA(PBE) [this work]	1.93	2.01	-0.28	5.56
VASP, PAW, GGA [17, 32-37]	(1.84 - 1.93)	(1.92 - 1.98)	(-0.12 - -0.14)	(5.52 - 5.72)
VASP, PW91, USPP-GGA [38]	1.95	1.99	-0.16	5.73
WIEN2K, FP-LAPW, GGA [39]	1.96	1.97	-0.13	5.76
QUANTUM ESPRESSO, PWscf, GGA [40]	2.04	2.09	-0.24	5.90
CASTEP, GGA [31, 41, 42]	(1.83 - 1.90)	(1.94 - 1.98)	(-0.24 - -0.23)	(5.55 - 5.56)
ortho-Co ₃ C				
	$m_s(\text{Co}^g)$	$m_s(\text{Co}^s)$	$m_s(\text{C})$	total m_s
FPLO, GGA(PBE) [this work]	1.12	1.02	-0.11	3.16
VASP, PAW, GGA [17, 37]	0.98	1.07	-0.05	(2.98 - 3.12)

TABLE II. The initial and optimized lattice parameters and Wyckoff positions for hexa-Fe₃C (s.g. $P6_322$) and ortho-Fe₃C (s.g. $Pnma$) phases. The geometry optimization was performed with the FPLO18 code using the PBE potential.

Initial structural data				
Phase	Space group	Lattice parameters	Wyckoff positions	
hexa-Fe ₃ C [55]	$P6_322$ (182)	$a = b = 4.767$	Fe = 0.333	0 0
		$c = 4.354$	C =	1/3 2/3 3/4
		$a = 5.092$	Fe ^g = 0.1834	0.0689 0.3344
ortho-Fe ₃ C [56]	$Pnma$ (62)	$b = 6.741$	Fe ^s = 0.0388	0.25 0.8422
		$c = 4.527$	C =	0.8764 0.25 0.4426
Optimized structural data				
Phase	Space group	Lattice parameters	Wyckoff positions	
hexa-Fe ₃ C	$P6_322$ (182)	$a = b = 4.677$	Fe = 0.3196	0 0
		$c = 4.344$	C =	1/3 2/3 3/4
hexa-Co ₃ C	$P6_322$ (182)	$a = b = 4.5497$	Co = 0.32348	0 0
		$c = 4.4095$	C =	1/3 2/3 3/4
ortho-Fe ₃ C	$Pnma$ (62)	$a = 5.0510$	Fe ^g = 0.1765	0.0664 0.3322
		$b = 6.6867$	Fe ^s = 0.0337	0.25 0.8392
		$c = 4.4906$	C =	0.8762 0.25 0.4381
ortho-Co ₃ C	$Pnma$ (62)	$a = 4.996$	Co ^g = 0.1805	0.0683 0.3314
		$b = 6.614$	Co ^s = 0.0372	0.25 0.8451
		$c = 4.442$	C =	0.8794 0.25 0.4479

the Wyckoff positions were optimized using forces. The choice of a substitution concentration of $\frac{1}{12}$ is based on the trade-off between the relatively low concentration value and the computation time. Within the supercell method, an alternative concentration of $\frac{1}{24}$ would have to be based on twice the elemental cell, which would increase calculation time by several times.

Formation energies (E_f) of Fe₁₁X₁C₄ alloys were calculated from equation:

$$E_f = E_{\text{Fe}_{11}\text{X}_1\text{C}_4} - 11E_{\text{Fe}} - E_X - 4E_C, \quad (1)$$

where $E_{\text{Fe}_{11}\text{X}_1\text{C}_4}$, E_{Fe} , E_C , and E_X are the total energies of the $\text{Fe}_{11}\text{X}_1\text{C}_4$ supercell and the crystals of iron, carbon (graphite), and transition metal (X), respectively.

To determine the total energies, we prepared and optimized the geometry of $3d$, $4d$, and $5d$ crystals. The formation energies of hexa- $\text{Co}_{11}\text{X}_1\text{C}_4$ compositions were calculated analogously.

For the hexagonal crystal system, the MAE can be estimated from the difference in energies calculated for magnetization along the unique crystal axis and the axis perpendicular to it. It can give both non-negative and negative values, for perpendicular and in-plane magnetocrystalline anisotropy, respectively.

Following our approach for calculating the MAE in orthorhombic structures [64], we have applied the same method in this work. The axis of easy magnetization is defined by the lowest energy of the three fully relativistic quantization directions along the main crystal axes ([100], [010], and [001] along a , b , and c , respectively). For each composition, we define an axis with the lowest energy (E_1), medium energy (E_2), and highest energy (E_3). The MAE of an orthorhombic system is determined by the difference between the medium and lowest energy, which gives us only non-negative MAE values. To complete the determination of MAE in the orthorhombic structure, we introduced the DE_{32} parameter describing the anisotropy energy between E_3 and E_2 . For the experimental determination of the effective MAE, similar approach was used by Zhdanova *et al.* [65].

Another key parameter when discussing permanent magnet applications is magnetic hardness [11], which can be expressed as :

$$\kappa = \sqrt{\frac{K}{\mu_0 M_s^2}}, \quad (2)$$

where K is magnetocrystalline anisotropy constant (interpreted as MAE), μ_0 is vacuum permeability, and M_s is saturation magnetization. The latter might be given as:

$$M_s = \frac{m_s + m_l}{V}, \quad (3)$$

where m_s is total spin magnetic moment, m_l is total orbital magnetic moment, and V is unit cell volume. It is assumed that $0.5 < \kappa < 1$ defines the range of semi-hard magnetic materials, while $\kappa > 1$ denotes hard magnetic materials.

Curie temperature (T_C^{MFT}) of $(\text{Fe}_{0.916}\text{X}_{0.084})_3\text{C}$ alloys with the $3d$, $4d$, and $5d$ transition metals (X) were calculated using mean-field theory [66, 67]. The $(\text{Fe}_{0.916}\text{X}_{0.084})_3\text{C}$ concentration, modeled here with coherent potential approximation (CPA), was chosen to match the $\text{Fe}_{11}\text{X}_1\text{C}_4$ concentration, modeled with supercell method. We used the:

$$k_B T_C^{\text{MFT}} = \frac{2}{3} \frac{E_{\text{DLM}} - E_{\text{FM}}}{c}, \quad (4)$$

equation. Here, E_{DLM} and E_{FM} are the total energies of the paramagnetic and ferromagnetic solutions, k_B is Boltzmann's constant, and c is the number of magnetic atoms in formula. For Fe_3C we assume c equal 3. To

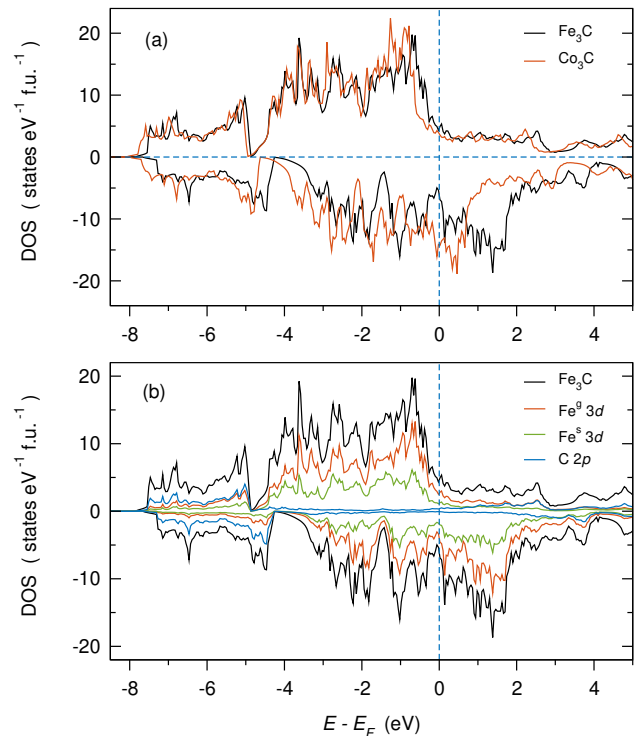


FIG. 2. Densities of states (DOS) for ortho- Fe_3C and ortho- Co_3C . The calculations were performed with the FPLO18 code using the PBE exchange-correlation potential.

TABLE III. Total spin magnetic moments [m_s (μ_B f.u. $^{-1}$)] and the magnetocrystalline anisotropy energies [MAE (MJ m^{-3})] calculated for hexa- Fe_3C , hexa- Co_3C , ortho- Fe_3C , and ortho- Co_3C . The equilibrium values were obtained using the von Barth and Hedin (vBH), Perdew and Zunger (PZ), Perdew and Wang 92 (PW92), Perdew-Burke-Ernzerhof (PBE), and LDA exchange-only (x-only) exchange-correlation potentials (V_{xc}). The calculations were performed with the FPLO code. At the first line, the VASP-PAW-PBE results from Ref. [17] are presented.

V_{xc}	hexa- Fe_3C		hexa- Co_3C		ortho- Fe_3C		ortho- Co_3C	
	m_s	MAE	m_s	MAE	m_s	MAE	m_s	MAE
PBE [17]	5.92	0.57	2.76	0.02	5.52	0.05	3.12	0.81
PBE	6.05	0.68	2.95	-0.15	5.56	0.11	3.16	0.67
vBH	5.40	0.55	2.48	0.26	4.88	0.24	2.76	0.81
PZ	5.40	0.55	2.48	0.26	4.88	0.24	2.77	0.81
PW92	5.66	0.71	2.67	0.02	5.16	0.35	2.89	0.88
x-only	6.36	0.41	3.20	0.03	5.88	0.05	3.38	0.72

model the paramagnetic configuration, we used the disordered local moment (DLM) approach [68] with the coherent potential approximation (CPA) [69]. Scalar-relativistic DLM-CPA calculations were conducted using the FPLO5 code, which is the most recent version of the FPLO code that incorporates CPA. However, the FPLO5 code lacks the PBE-GGA implementation, forcing the use of the LDA-PW92 exchange-correlation potential for CPA calculations [63].

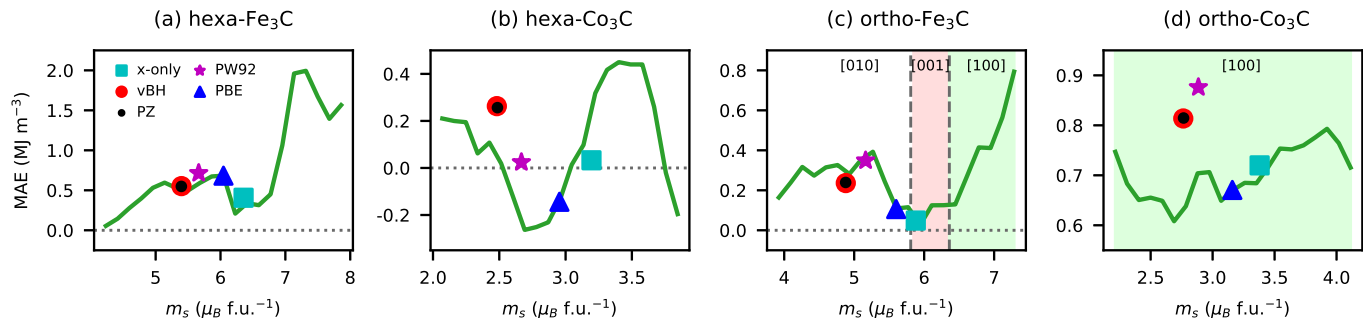


FIG. 3. The dependence of the magnetocrystalline anisotropy energy (MAE) on the spin magnetic moment (m_s) for (a) hexa- Fe_3C , (b) hexa- Co_3C , (c) ortho- Fe_3C , and (d) ortho- Co_3C . The calculations were performed with the FPLO18 code using the Perdew-Burke-Ernzerhof (PBE) exchange-correlation potential. Equilibrium values of MAE and m_s were obtained using functionals of von Barth and Hedin (vBH), Perdew and Zunger (PZ), Perdew and Wang 92 (PW92), and LDA exchange-only (x-only), besides Perdew-Burke-Ernzerhof (PBE) in the generalized gradient approximation (GGA). They are represented by symbols. The structures with different axes of easy magnetization are distinguished by different background colors: white for [010], light red for [001], and light green for [100]. In the case of ortho- Co_3C there is one easy axis for the whole considered range of magnetic moments, namely [100].

III. RESULTS AND DISCUSSION

This paper consists of four parts. In the first, we discuss Fe_3C and Co_3C compounds. In the second, the $(\text{Fe},\text{Co})_3\text{C}$ alloys. In the third, transition metal substitutions in Fe_3C and Co_3C compounds. In the fourth, B and N substitutions at the C position in $(\text{Fe},\text{Co})_3\text{C}$ alloys. Each time, we consider both hexagonal and orthorhombic phases.

III.1. Fe_3C and Co_3C compounds

In this section, dedicated to the Fe_3C and Co_3C compounds, we will present their densities of states, examine how the choice of the exchange-correlation potential affects the obtained values of magnetic moments and magnetocrystalline anisotropy energy (MAE), and study the dependence of MAE on the magnetic moment. We started this study from the geometry optimization of considered phases, and the optimized structural parameters are presented in Table II.

The calculated formation energies are positive for all four compounds considered in this section (hexa- Fe_3C , hexa- Co_3C , ortho- Fe_3C , and ortho- Co_3C), indicating their instability, which agrees with experimental formation enthalpies [70] and previous computational results [17, 19, 33]. Orthorhombic phases have slightly lower energies than hexagonal ones, suggesting that Fe_3C and Co_3C will prefer the cementite-type structure. The formation energies are also relatively low, giving the possibility of stabilizing the compounds with additional factors such as alloying or the presence of a second phase. Nanoparticles of ortho- Co_3C were successfully synthesized [13, 71] and the bulk form of ortho- Co_3C has been obtained under high pressure (above 4.8 GPa) [19]. Another method of stabilizing ortho- Co_3C is its alloying with a stable isostructural Co_3B phase [72].

Figure 2 presents the densities of states (DOS) calculated for orthorhombic Fe_3C and Co_3C . Densities of states for hexagonal phases look very similar to orthorhombic, and we decide to not show them. The valence band of ortho- Fe_3C is dominated by Fe 3d and C 2p orbitals, between which a clear hybridization is visible. The spin polarization of the valence band is noticeably stronger for Fe_3C .

The total spin magnetic moments, corresponding to the spin polarization in the DOS, are 5.56 and 3.16 $\mu_B \text{ f.u.}^{-1}$ for ortho- Fe_3C and ortho- Co_3C , respectively. The values of calculated total and partial spin magnetic moments are summarized in the Table IV. In the Table I, we have further compared our results (obtained with the full-potential PBE approach) with those from the literature. Given the differences in the calculation methods used, we rate the level of agreement as good. Later, we will discuss how the choice of exchange-correlation potential affects the spin magnetic moment.

The spin magnetic moment on the Fe atom, determined in our PBE calculations, shows a higher value for hexa- Fe_3C (2.12 μ_B) and lower values for ortho- Fe_3C phase (1.93 and 2.01 μ_B for general and special Fe positions, respectively). All values are smaller than the magnetic moments for bcc Fe (2.17 μ_B [73] or 2.20 μ_B [74]). In contrast, the hexa- Co_3C phase exhibits smaller spin magnetic moments on Co atoms (1.02 μ_B) than the ortho- Co_3C phase (1.02 and 1.12 μ_B for special and general Co positions, respectively). The m_s values for bulk fcc Co are higher (1.66 μ_B [73]; 1.58 μ_B [75]) than those calculated for Co_3C .

In the present work, our aim is not to repeat the calculation of magnetic moments, which, as we see in the Table I, has already been done, but to calculate the magnetocrystalline anisotropy energies (MAE) and determine magnetic hardness of considered materials. The MAE values calculated with PBE functional (at 0 K) are 0.68, -0.14, 0.11, and 0.67 MJ m^{-3} for hexa- Fe_3C , hexa- Co_3C , ortho- Fe_3C and ortho- Co_3C , respec-

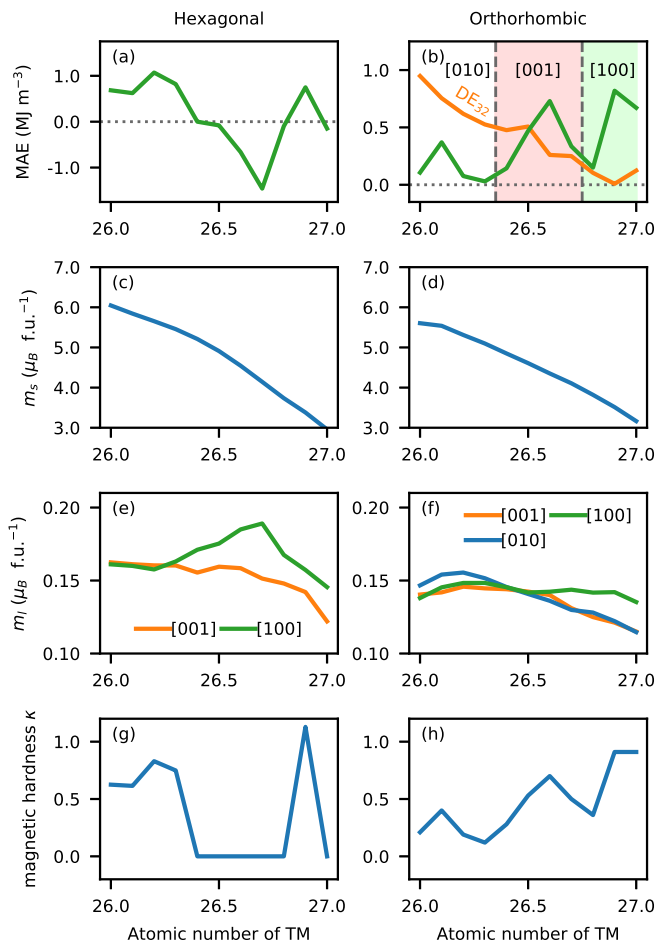


FIG. 4. Intrinsic properties calculated for hexa- and ortho- $(\text{Fe}_{1-x}\text{Co}_x)_3\text{C}$ alloys. The increase in Co concentration x is expressed as an increase in the atomic number of the transition metal (TM) element; from 26 (Fe) to 27 (Co). (a, b) The magnetocrystalline anisotropy energy (MAE) is represented by the green line, and the energy difference between the two higher energies of three energies calculated for three orthogonal magnetization directions ($\text{DE}_{32} = E_3 - E_2$) by the orange line. (c-f) The total spin (m_s) and orbital (m_l) magnetic moments, and (g, h) the magnetic hardness (κ). The concentration range for panel (b) is divided into regions characterized by the magnetic easy axes. Calculations were performed with the virtual crystal approximation (VCA) using the FPLO18 code with PBE exchange-correlation potential.

tively, see Table III. The calculated MAE of ortho- Co_3C is in agreement with experimental magnetocrystalline anisotropy constant determined for ortho- Co_3C nanoparticles as $0.74 \pm 0.1 \text{ MJ m}^{-3}$ [23]. The corresponding MAE values calculated within projector augmented wave PBE method are 0.57, 0.02, 0.05, and 0.81 MJ m^{-3} for hexa- Fe_3C , hexa- Co_3C , ortho- Fe_3C and ortho- Co_3C , respectively [17], please check Table III. The similarity between two sets of computational results is qualitatively good, whereas the quantitative differences come most probably from the shape approximation of the potential used by Wu *et al.* [17]. Another theoretical approach determines MAE of ortho- Co_3C as between 0.8 and 0.9 MJ m^{-3} [23],

TABLE IV. Calculated magnetic properties of hexagonal and orthorhombic $(\text{Fe}_{1-x}\text{Co}_x)_3\text{C}$ alloys. Spin and orbital magnetic moments [m_s and m_l (μ_B per atom or f.u.)], magnetocrystalline anisotropy energy [MAE (MJ m^{-3})], and magnetic hardness [κ]. Magnetic moments on transition-metal (TM) elements for ortho- $(\text{Fe}_{1-x}\text{Co}_x)_3\text{C}$ alloys are given for both general and special non-equivalent crystallographic sites. The increase in Co concentration x is expressed as an increase in the atomic number of the transition metal (TM) element; from 26.0 for Fe to 27.0 for Co. The calculations were performed with the FPLO18 code using the PBE potential and virtual crystal approximation.

Hexagonal	Atomic number of TM				
	26.0	26.2	26.7	26.9	27.0
$m_s(\text{Fe/Co})$	2.12	1.97	1.44	1.17	1.03
$m_s(\text{C})$	-0.30	-0.27	-0.18	-0.14	-0.12
total m_s	6.04	5.65	4.14	3.38	2.95
$m_l(\text{Fe/Co})$	0.053	0.052	0.049	0.046	0.040
$m_l(\text{C})$	0.00	0.00	0.00	0.00	0.00
total m_l	0.16	0.16	0.15	0.14	0.12
MAE	0.68	1.07	-1.46	0.75	-0.15
κ	0.63	0.83	0.00	1.13	0.00
Orthorhombic	Atomic number of TM				
	26.0	26.1	26.6	26.9	27.0
$m_s(\text{Fe}^g/\text{Co}^g)$	1.93	1.90	1.52	1.24	1.12
$m_s(\text{Fe}^s/\text{Co}^s)$	2.01	1.99	1.47	1.14	1.02
$m_s(\text{C})$	-0.28	-0.26	-0.18	-0.12	-0.11
total m_s	5.56	5.53	4.34	3.51	3.16
$m_l(\text{Fe}^g/\text{Co}^g)$	0.042	0.044	0.038	0.035	0.034
$m_l(\text{Fe}^s/\text{Co}^s)$	0.054	0.055	0.050	0.048	0.043
$m_l(\text{C})$	0.00	0.00	0.00	0.00	0.00
total m_l	0.14	0.14	0.14	0.12	0.12
MAE	0.11	0.37	0.73	0.82	0.67
κ	0.21	0.40	0.70	0.91	0.91

identifying ortho- Co_3C phase as hard magnetic. Since all the mentioned results are calculated for a temperature of 0 K and additionally depend on the approximation used, they should be interpreted with due caution. In order to establish a context for the PBE-MAE results, we will present an analysis of the impact of the form of exchange-correlation potential on the MAE values and the relation between values of MAE and spin magnetic moment.

In our previous works, we demonstrated that the calculated MAE values for CeFe_{12} and MnB depend on the choice of the exchange-correlation potential [64, 76]. We also showed there, that the MAE is correlated with the spin magnetic moment (m_s). Here, we performed MAE and m_s calculations for the Fe_3C and Co_3C compounds using five forms of exchange-correlation potential: Perdew-Burke-Ernzerhof (PBE), von Barth and Hedin (vBH), Perdew and Zunger (PZ), Perdew and Wang 92 (PW92), and LSDA exchange only (x-only). The self-consistent equilibrium results of MAE and m_s are shown in Fig. 3, and in Table III. For each phase, the calculated magnetic moment increases going from vBH

and PZ, through PW92, PBE, to the x -only potential. In the case of MAE, there is a scattering of results with a range of up to about 0.4 MJ m^{-3} . However, we do not observe any clear trends in the MAE values. In contrast, the magnetic moments increase in each case with the following order of exchange-correlation potentials: $v\text{BH}/\text{PZ} \rightarrow \text{PW92} \rightarrow \text{PBE} \rightarrow x\text{-only}$. In the case of referred ortho- Co_3C , alternative functionals result in MAE values that are even higher than those obtained with PBE. Thus, ortho- Co_3C appears to be a promising hard-magnetic material, regardless of the approximation used.

Furthermore, we performed calculations of the dependencies of MAE on the fixed spin magnetic moment (FSM), see Fig. 3. We observe, that the dependencies of MAE on fixed spin magnetic moment overlap with equilibrium data points calculated with different functionals.

For hexa- Fe_3C , in the whole range of magnetic moments, we observe positive MAE values, implying uniaxial magnetocrystalline anisotropy. The MAE ranges from about 0 to 2 MJ m^{-3} . Unfortunately, while lowering the magnetic moment of the system is a relatively straightforward task, engineering an increase in the magnetic moment of Fe_3C can be difficult. It is because Fe_3C has one of the highest magnetic moments among isostructural compounds, and Fe substitution by both Mn and Co leads to a lower magnetic moment.

The magnetic moment of Co_3C phases is about half that of Fe_3C phases. For hexa- Co_3C , with increasing magnetic moment, we observe both positive and negative values of MAE, which indicate changes between easy-axis and easy-plane types of magnetocrystalline anisotropy, respectively. All MAE values determined for hexa- Co_3C phase classify it as a magnetically soft material.

In the case of ortho- Fe_3C we observe somewhat lower equilibrium magnetic moments than for hexa- Fe_3C . For ortho- Fe_3C , with increasing magnetic moment, the axis of easy magnetization undergoes a change from [010] to [001] and subsequently to [100]. The calculated equilibrium MAE values range from 0.05 to 0.35 MJ m^{-3} . For the highest considered magnetic moments, above $7 \mu_{\text{B}} \text{ f.u.}^{-1}$, the MAE increases up to 0.8 MJ m^{-3} . Unfortunately, as we have already said for hexa- Fe_3C counterpart, raising the magnetic moment of ortho- Fe_3C might be a difficult task. While previous experiments on $\text{Fe}_3(\text{B,C})$ borocarbides have demonstrated that substituting C by B can result in an approximate 10% increase in the magnetic moment of the system [21], this would still not be sufficient to reach the high MAE range.

In the ortho- Co_3C system, the obtained PBE-MAE values vary only slightly with the change of the spin magnetic moment, from 0.6 to 0.8 MJ m^{-3} . The equilibrium MAE values calculated in LDA ($v\text{BH}$, PZ, and PW92) exceed this range and reach 0.9 MJ m^{-3} . As we said already in the previous section, the calculated MAE of ortho- Co_3C is in agreement with experimental magnetocrystalline anisotropy constant determined for ortho- Co_3C nanoparticles as $0.74 \pm 0.1 \text{ MJ m}^{-3}$ [23]. Since the observed MAE values are relatively high and the mag-

netic moments are low, the magnetic hardness is close or above one for the whole considered range of fixed spin magnetic moments.

In summary, from the perspective of magnetic hardness, the ortho- Co_3C phase deserves the most attention. Calculations suggest that magnetic hardness close to unity should persist not only at 0 K, but also at room temperature when the magnetic moment decreases. Having determined the magnetic hardness of Fe_3C and Co_3C compounds, in the next section we will address the full ranges of intermediate concentrations of $(\text{Fe,Co})_3\text{C}$ alloys.

III.2. $(\text{Fe,Co})_3\text{C}$ alloys

Since Fe and Co have consecutive atomic numbers of 26 and 27, their alloys can be modeled using a virtual atom with a fractional atomic number determined by the concentration of the elements. Our goal is to study how the MAE of the system changes with Co concentration and identify promising compositions with elevated MAE. In our attempt we are motivated by previous studies, such as for FeCo , $(\text{Fe,Co})_2\text{B}$ and $(\text{Fe,Co})_{16}\text{C}$ alloys [77–79], which showed higher MAE values for intermediate compositions than for compounds at the extremes of the Fe/Co range. Moreover, we will determine how the spin and orbital magnetic moments change with Co concentration.

At first, we analyze the concentration dependence of MAE of the hexa- $(\text{Fe,Co})_3\text{C}$ phase, see Fig. 4(a) and Table IV. We observe both positive and negative MAE values, indicating uniaxial and in-plane magnetocrystalline anisotropies, respectively. The highest MAE of 1.07 MJ m^{-3} was obtained for a concentration of 20% Co, and the minimum MAE of -1.46 MJ m^{-3} for 70% Co. This trend is not surprising, as an analogous course of $\text{MAE}(x)$ with a positive maximum and a negative minimum was observed for the mentioned before $(\text{Fe}_{1-x}\text{Co}_x)_2\text{B}$ and $(\text{Fe}_{1-x}\text{Co}_x)_{16}\text{C}$ alloys [78, 79].

For ortho- $(\text{Fe,Co})_3\text{C}$ alloys, the Co concentration range is divided into regions: from 0% to 35%, from 35% to 75%, and from 75% to 100%, with the directions of magnetic easy axes [010], [001], and [100], respectively, see Fig. 4(b). The highest MAE value of 0.82 MJ m^{-3} was obtained for a concentration of 90% Co. Additionally, for orthorhombic alloys, we show the energy difference between two higher energies ($\text{DE}_{32} = E_3 - E_2$) complementing the MAE. The low DE_{32} values, as observed for Co-rich phases, strengthen the uniaxial character of the magnetocrystalline anisotropy of these systems.

Wu *et al.* synthesized a sample of Fe_2CoC and measured the MAE for it at 10 K as 0.96 MJ m^{-3} [17]. In contrast, our calculations for about 1/3 Co concentration indicate MAE close to zero. Such a discrepancy may be due to the limitations of the VCA method used and the high value of DE_{32} , but also to the presence of other phases in the experimental sample and the influence of the microstructure on the result measured. Nevertheless,

the relatively high experimental MAE value encourages further exploration of magnetically hard materials in the cementite family.

The total spin magnetic moment (m_s) is highest for the terminal Fe_3C phases for both hexagonal and orthorhombic structures, and decrease with Co concentration, see Figs. 4(c,d). We do not observe a pronounced maximum in the intermediate range. This behavior is similar to that observed, for example, for Fe/Co monoborides [64].

For $(\text{Fe},\text{Co})_3\text{C}$ alloys, we observe significant differences in the total orbital magnetic moments (m_l) determined for various crystallographic directions, see Figs. 4(e,f). Although in some cases orbital moment differences correlate with magnetocrystalline anisotropy, this time we do not observe such relation. The calculated orbital magnetic moments, see Table IV, on the Fe sites of 0.04–0.05 μ_B are close to the value calculated for bcc Fe of 0.045 μ_B [73]. However, both calculated values underestimate the experimental orbital magnetic moment in bcc Fe of 0.086 μ_B [80]. The m_l values calculated for Co_3C phases are lower than the corresponding values for Fe_3C phases. Moreover, the m_l values determined for Co_3C are lower than the values for fcc Co of 0.071 μ_B [75] and 0.073 μ_B [73].

Hexagonal $(\text{Fe},\text{Co})_3\text{C}$ alloys with Co concentration from 0 to 30% are magnetically semi-hard ($0.5 < \kappa < 1$), see Fig.4(g). For negative values of MAE, seen in the center of the concentration range, we assumed $\kappa = 0$, see Table IV. The hexagonal carbide with 90% Co indicates $\kappa = 1.13$, which defines it as magnetically hard.

For orthorhombic alloys, see Fig.4(h), semi-hard magnetic properties are observed for most of Co concentrations above 50%.

III.3. Fe_3C and Co_3C alloys with transition metals

In this section, we will discuss calculation results for Fe_3C and Co_3C alloys with transition metals. In our models, the transition metal atom replaces one of the twelve Fe (or Co) atoms in the $\text{Fe}_{11}\text{X}_1\text{C}_4$ (or $\text{Co}_{11}\text{X}_1\text{C}_4$) supercell, see Fig. II. Similar models of ortho- $\text{Fe}_{11}\text{X}_1\text{C}_4$ alloys have been investigated by Shein *et al.* [33]. Below we will present the results of calculations of formation energies, magnetic moments, and magnetocrystalline anisotropy energies. These results are further complemented by Curie temperature calculations performed using the disorder local moments (DLM) method. In the following analysis, we consider hexa- Fe_3C , ortho- Fe_3C , and ortho- Co_3C alloys, ignoring hexa- Co_3C alloys. The decision to exclude hexa- Co_3C alloys is due to the unpromising properties of the hexa- Co_3C compound (magnetic hardness equal zero and formation energy higher than for ortho- Co_3C phase).

III.3.1. Formation energy

Figure 5 presents the calculated formation energies for hexa- Fe_3C , ortho- Fe_3C , and ortho- Co_3C alloys with transition metals. With one exception (ortho- $\text{Fe}_{11}\text{Ti}_1\text{C}_4$), all alloys have positive formation energies, implying lack of chemical stability. The positive values are in most cases relatively small, making it possible to stabilize the materials by forming nanoparticles, alloys, or composites [17, 21, 27, 45].

The calculated formation energy of hexa- Fe_3C is about 0.085 eV atom⁻¹ and is slightly higher than that for ortho- Fe_3C (0.055 eV atom⁻¹). The situation is similar when comparing trends for hexa- Fe_3C and ortho- Fe_3C alloys with transition metals. The calculated formation energy of ortho- Fe_3C (0.055 eV atom⁻¹) stays in a good agreement with previous theoretical and experimental results (0.05–0.08 eV atom⁻¹) [33, 45, 50]. The plots of dependencies of formation energies on 3d and 4d transition metal substitutions in ortho- Fe_3C are almost identical to the previously mentioned theoretical results [33, 50]. Although the formation energies of the alloys studied provide valuable information, the idealized single-phase nature of the models means that the actual impact of additives is best verified experimentally. Bulk ortho- Fe_3C has been tested by Umemoto *et al.* [27], who found that additions of Cr, Mn, V and Mo additions stabilize the cementite, whereas Ti, Ni, and Si destabilize it. Furthermore, it has been determined that the substitution of 5 at.% Ti leads to the appearance of additional phases of TiC and $\alpha\text{-Fe}$ [27]. The formation energies of ortho- Co_3C alloys are higher than those of ortho- Fe_3C , however, still relatively low.

III.3.2. Curie temperature

From the standpoint of potential applications of the material in permanent magnets, it is important that its Curie temperature far exceeds the room temperature. For metastable hexa- Fe_3C , the Curie temperature is difficult to determine and only an approximate experimental value of $T_C \geq 653$ K is given [81]. Whereas, off-stoichiometric hexa- $\text{Fe}_{2.2}\text{C}$ has T_C of about 723 K [82]. Experimental Curie temperatures of ortho- Fe_3C and ortho- Co_3C are about 481 K [21] and 650 K [23], respectively. In Fig. 6 we present the mean-field theory Curie temperatures (T_C^{MFT}) calculated for hexa- $(\text{Fe}_{0.916}\text{X}_{0.084})_3\text{C}$, ortho- $(\text{Fe}_{0.916}\text{X}_{0.084})_3\text{C}$, and ortho- $(\text{Co}_{0.916}\text{X}_{0.084})_3\text{C}$ alloys with transition metals X. The transition metal concentration of 0.084 was chosen to reproduce the $\frac{1}{12}$ concentration of transition metal element X in $\text{Fe}_{11}\text{X}_1\text{C}_4$ models.

The calculated T_C for hexa- Fe_3C is 1040 K, which is much higher than the mentioned experimental estimation ($T_C \geq 653$ K). The observed difference in T_C may come from both the known overestimation of T_C in the mean-field theory and the underestimation of the experimental value. In Fig. 6 we see, that the dependencies

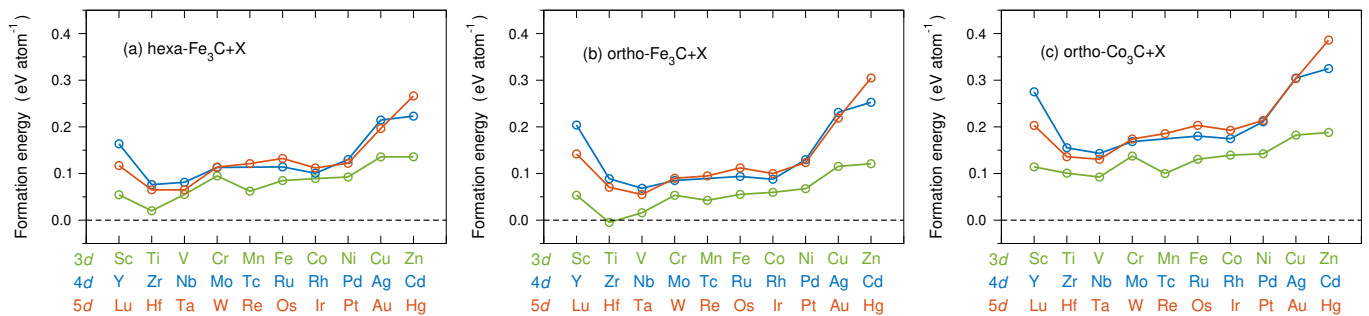


FIG. 5. Formation energies for (a) hexa- Fe_3C , (b) ortho- Fe_3C , and (c) ortho- Co_3C alloys with $3d$, $4d$, and $5d$ transition metals X [$(\text{Fe}/\text{Co})_{11}\text{X}_1\text{C}_4$]. The calculations were performed with FPLO18 code using the PBE functional and supercell approach.

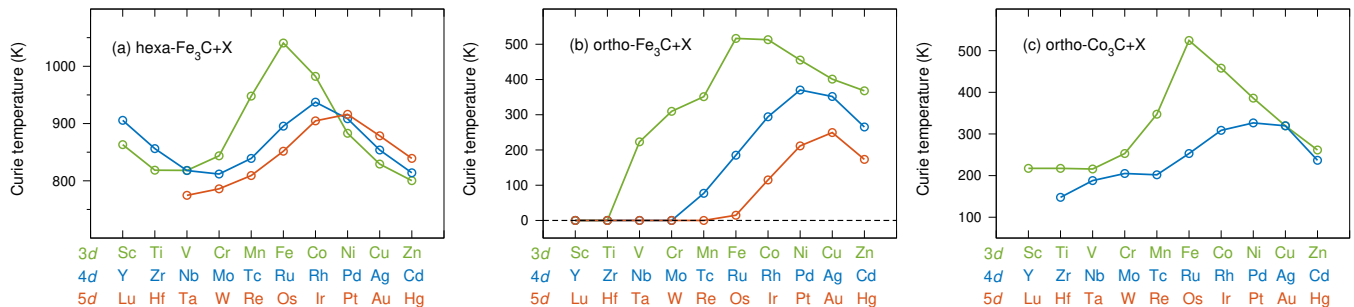


FIG. 6. The mean-field-theory Curie temperatures (T_C^{MFT}) for hexa- and ortho- $(\text{Fe}_{0.916}\text{X}_{0.084})_3\text{C}$ alloys with $3d$, $4d$, and $5d$ transition metals X . The results were calculated using the FPLO5 code and the Perdew and Wang (PW92) functional. The chemical disorder was modeled with coherent potential approximation (CPA) and the paramagnetic state with disorder local moment (DLM-CPA) method. For ortho- Fe_3C and ortho- Co_3C phases, the experimental Curie temperatures are 481 K [21] and about 650 K [23], respectively.

of T_C on the atomic number of substitution have a clear sinusoidal trend and that each substitution reduces the T_C of the parental hexa- Fe_3C compound. Nevertheless, all the considered hexa- $\text{Fe}_3\text{C} + \text{X}$ alloys show relatively high T_C .

Calculated T_C of ortho- Fe_3C is equal to 516 K, in good agreement with experimental value of 481 K [21]. Calculated trends for transition metal elements suggest that all substitutions, except Co, will significantly reduce the T_C of the alloy. Whereas, the elements $4d$ and $5d$ will have stronger effect than the elements $3d$. The transition metal elements on the left side of the periods reduce T_C to zero, which means the absence of magnetic ordering. Previous experiments confirm the reduction of Curie temperature after alloying of cementite with Cr, Mn, or Mo [25, 26]. However, it has been measured that up to about 2% Ni raises the Curie temperature of the cementite [25]. The effect of lowering T_C can make it difficult or impossible to use most transition metals as additives to affect MAE and magnetic hardness. The solution could be, for example, a combination of transition metal alloying on the Fe site with B alloying on the C side. Indeed, the experiment showed a linear growth in T_C up to 851 K with increasing B concentration in ortho- $\text{Fe}_3(\text{B},\text{C})$ borocarbides [21].

Calculated T_C of ortho- Co_3C is equal to 458 K, whereas experimental T_C of Co_3C -based nanoparticles have been determined as 510 K [83], 563 K [84], or

650 K [23]. Calculations indicate that only Fe substitution raises the T_C of the ortho- Co_3C -based system, while all other elements considered lower it. The determined T_C values below and well below 400 K suggest the impossibility of using most ortho- $\text{Co}_3\text{C} + \text{X}$ alloys as permanent magnets. The solution, as we suggested above, could be the alloying of B at the C position, since, as shown experimentally, the T_C of ortho- Co_3B is much higher than the value for ortho- Co_3C and is 750 K [16].

III.3.3. Magnetic moments and magnetic hardness

After discussing the formation energy and Curie temperature, we will show how alloying with transition metals affect the magnetic moments and magnetic hardness, see Figs. 7, 8, and 9 for hexa- $\text{Fe}_{11}\text{X}_1\text{C}_4$, ortho- $\text{Fe}_{11}\text{X}_1\text{C}_4$, and ortho- $\text{Co}_{11}\text{X}_1\text{C}_4$ alloys, respectively. In the majority of instances, clear patterns emerge with regard to the dependencies. Trends in magnetic moments are similar to those calculated previously for alloys of ortho- Fe_3C [33], CeFe_{12} [76], monoborides [64], and Fe [85–87]. MAE trends, on the other hand, do not resemble previous findings.

III.3.3.1. Hexa- Fe_3C alloys with transition metals

We will begin our discussion of the results with hexa- Fe_3C alloys. Figure 7 presents a collection of the mag-

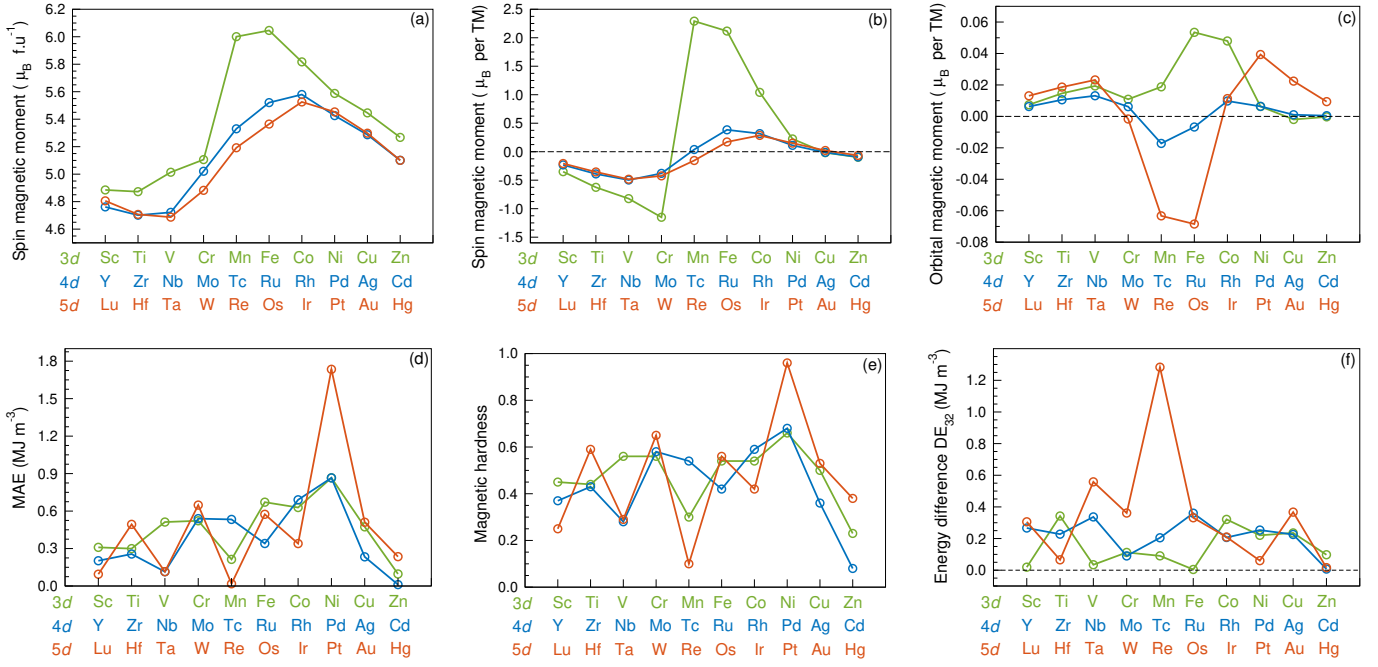


FIG. 7. The magnetic properties of hexa- Fe_3C alloys with $3d$, $4d$, and $5d$ transition metals X ($\text{Fe}_{11}\text{X}_1\text{C}_4$): (a) total spin magnetic moment (per formula unit); (b, c) spin and orbital magnetic moments on substitution atoms X (per TM atom); (d) magnetocrystalline anisotropy energy (MAE); (e) magnetic hardness; and (f) energy difference (DE_{32}) between the two higher energies among the three total energies calculated along the three main crystallographic axes. The calculations were performed with FPLO18 code using the PBE functional and supercell approach.

netic properties for alloys with $3d$, $4d$ and $5d$ metals. The spin magnetic moment trends for the three series of transition metals have a waveform shape, see Figs. 7(a,b). The parent system without substitution, hexa- Fe_3C , shows the highest total spin magnetic moment. All transition metal substitutions are spin polarized in the ferromagnetic medium and contribute to the total magnetic moment of the alloy, lowering its value. The orbital magnetic moments on the substitution sites are much smaller from spin magnetic moments, and oscillate between -0.07 and $+0.06 \mu_{\text{B}} \text{atom}^{-1}$, see Fig. 7(c).

Figures 7(d) and 7(f) show the magnetocrystalline anisotropy energies (MAE and DE_{32}) for hexa- $\text{Fe}_{11}\text{X}_1\text{C}_4$ alloys. From all considered compositions, the system with Pt has the highest MAE of 1.73 MJ m^{-3} . This value corresponds to the highest magnetic hardness of 0.96 , see Fig. 7(e). Our previous results for transition metal alloying in the Fe matrix, also pointed to Pt as a metal that stands out for its exceptionally positive effect on MAE [87]. Unfortunately, the high price of platinum, is not in favor of potential applications.

III.3.3.2. Ortho- Fe_3C alloys with transition metals

Trends of magnetic moments for ortho- Fe_3C alloys with transition metal elements, see Fig. 8(a-c), are similar to those presented above for hexa- Fe_3C alloys. However, the values of total spin magnetic moments are lower by about $0.5 \mu_{\text{B}} \text{f.u.}^{-1}$. Similar trends in local magnetic moments on transition metal substitutions were also observed in previous calculations for ortho- $\text{Fe}_{11}\text{X}_1\text{C}_4$ alloys with $3d$

and $4d$ elements [33]. Among the ortho- $\text{Fe}_{11}\text{X}_1\text{C}_4$ alloys, the parent ortho- Fe_3C compound has the highest total spin magnetic moment of $5.60 \mu_{\text{B}} \text{f.u.}^{-1}$.

The MAE and magnetic hardness of ortho- Fe_3C alloys appear more promising than that of hexa- Fe_3C alloys, see Fig. 8(d,e). The MAE increases above 1 MJ m^{-3} for Re, Ir, and Pt substitutions, leading to MAE values of 1.4 , 1.2 , and 1.1 MJ m^{-3} , respectively. However, as shown in Fig. 8(e), none of the alloys can be classified as a hard magnetic ($\kappa > 1$). The magnetic hardness closest to exceeding unity (0.93) has an alloy with Re. In addition, as we showed earlier, alloying ortho- Fe_3C with $5d$ transition metals leads to a strong decrease in Curie temperature. It makes the system with Re ultimately not a good candidate for a permanent magnet either.

In systems (such as orthorhombic) that do not have a unique distinguished crystallographic axis, we must be careful when considering MAE values, checking DE_{32} , see Sec. II for definition. The DE_{32} equal to 0.8 MJ m^{-3} for ortho- $\text{Fe}_{11}\text{Re}_1\text{C}_4$ with MAE of 1.4 MJ m^{-3} suggests uniaxial magnetocrystalline anisotropy. On the other hand, DE_{32} of around 2.4 MJ m^{-3} for ortho- $\text{Fe}_{11}\text{Os}_1\text{C}_4$, compared to MAE of 0.4 MJ m^{-3} suggests magnetocrystalline anisotropy close to easy-plane.

III.3.3.3. Ortho- Co_3C alloys with transition metals

The magnetic hardness of the ortho- Co_3C is one of the highest among the considered orthorhombic compositions, see Fig. 4. The magnetic properties calculated for ortho- Co_3C alloys are shown in Fig. 9. For the total spin

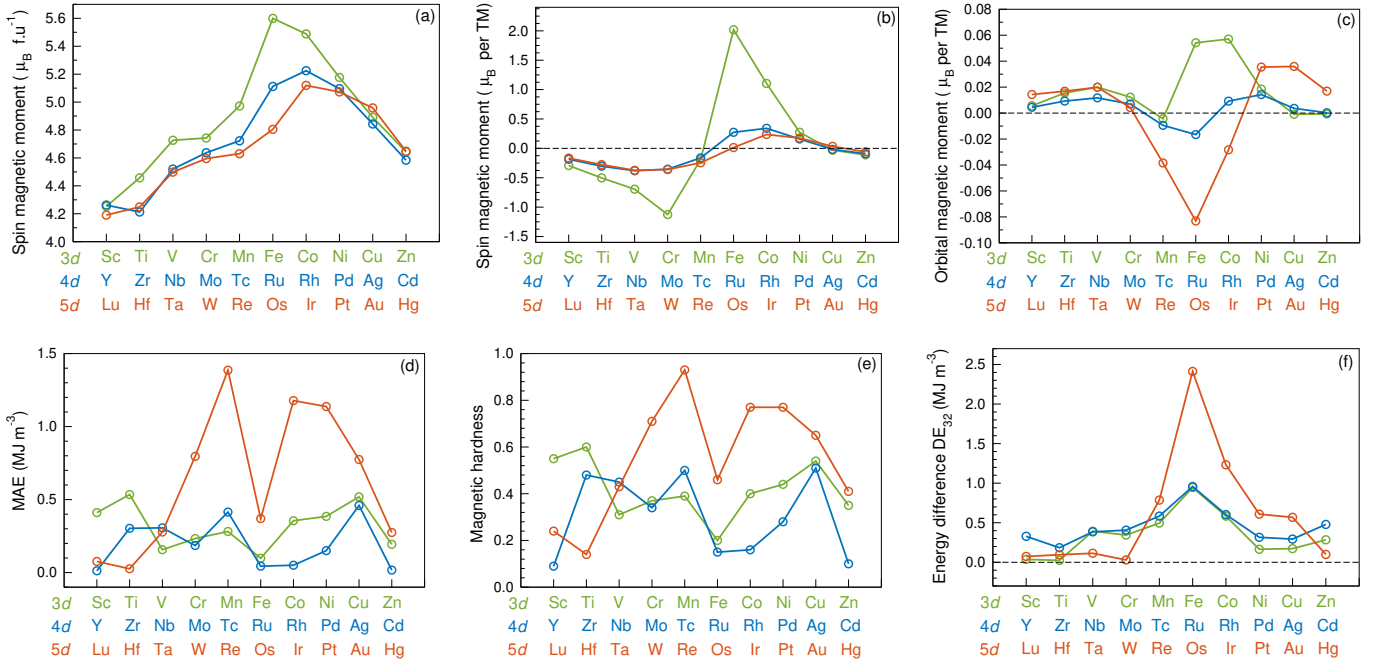


FIG. 8. The magnetic properties of ortho- Fe_3C alloys with 3d, 4d, and 5d transition metals X ($\text{Fe}_{11}\text{X}_1\text{C}_4$): (a) total spin magnetic moment (per formula unit); (b, c) spin and orbital magnetic moments on substitution atoms X (per TM atom); (d) magnetocrystalline anisotropy energy (MAE); (e) magnetic hardness; and (f) energy difference (DE_{32}) between the two higher energies among the three total energies calculated along the three main crystallographic axes. The calculations were performed with FPLO18 code using the PBE functional and supercell approach.

magnetic moment, see Fig. 9(a), we observe sinusoidal behavior, like before for hexa- Fe_3C alloys. However, the total magnetic moments calculated for ortho- Co_3C alloys are about half those for Fe_3C alloys. The maximum of spin magnetic moment, for $\text{Co}_{11}\text{Mn}_1\text{C}_4$, is equal to $3.4 \mu_B$ per f.u. and the minimum, for $\text{Co}_{11}\text{W}_1\text{C}_4$, is equal to $2.2 \mu_B$ per f.u. Only for Mn and Fe substitutions, the spin magnetic moment is higher than for Co in the initial ortho- Co_3C phase, see Fig. 9(b). The orbital magnetic moments on the substituted sites, ranging from -0.04 to $+0.04 \mu_B \text{ atom}^{-1}$, are also about twice smaller than in the case of Fe_3C alloys, see Fig. 9(c).

In Figure 9(d), we see once again that the MAE significantly depends on the substituting element. The calculated MAE results take a range from zero to 0.8 MJ m^{-3} . The MAE and magnetic hardness calculations indicate that $\text{Co}_{11}\text{W}_1\text{C}_4$ and $\text{Co}_{11}\text{Os}_1\text{C}_4$ can be classified as hard magnetic ($\kappa > 1$) with MAE values equal to 0.5 and 0.8 MJ m^{-3} , respectively, see Figs. 9(d,e). Unfortunately, as for ortho- $\text{Fe}_3\text{C} + \text{X}$ alloys, 5d substitutions will strongly lower the Curie temperature, making their use impractical. Alloying of ortho- Co_3C with transition metals in most cases causes a decrease in magnetic hardness. The small increase in magnetic hardness predicted for alloying with W and Os is burdened by the high prices of these elements and expected significant decrease in Curie temperature.

In summary, calculations of Curie temperature and magnetic hardness do not suggest that alloying with transition metals of hexa- Fe_3C , ortho- Fe_3C , and ortho- Co_3C

compounds lead to a significant improvement in their potential for permanent magnet applications. The magnetic hardness of hexa- $\text{Fe}_3\text{C} + \text{X}$ alloys, except for Pt substitution, does not exceed 0.7, and in addition, the formation energies of hexagonal alloys are higher than those of orthorhombic alloys, making them difficult to obtain. In the case of ortho- $\text{Fe}_3\text{C} + \text{X}$ alloys, Re, Ir, and Pt lead to an increase in magnetic hardness but at the same time lower the Curie temperature to values far below room temperature, which disqualifies potential applications for permanent magnets. In the case of the most promising hard magnetic ortho- Co_3C compound, a few 5d transition metals (Re, Pt, Au) do lead to a slight increase in magnetic hardness, but at the price of a significant drop in Curie temperature.

III.4. $(\text{Fe,Co})_3(\text{B,C,N})$ alloys

In Sec. III.2 we discussed $(\text{Fe/Co})_3\text{C}$ alloys in which substituting takes place at the 3d sites (Fe and Co). An additional degree of freedom in controlling the composition of Fe_3C -type alloys is substituting at the 2p (carbon) site [21, 53, 88]. Two natural candidates for such alloying are boron and nitrogen – carbon’s neighbors in the periodic table. Although $\text{Fe}_3(\text{B,C})$ borocarbides have been synthesized since at least the 1950s [21], they have not received wider attention. However, replacing carbon with boron in $\text{Fe}_3(\text{B,C})$ alloys leads to significant changes in properties. Nicholson showed experimentally that in the

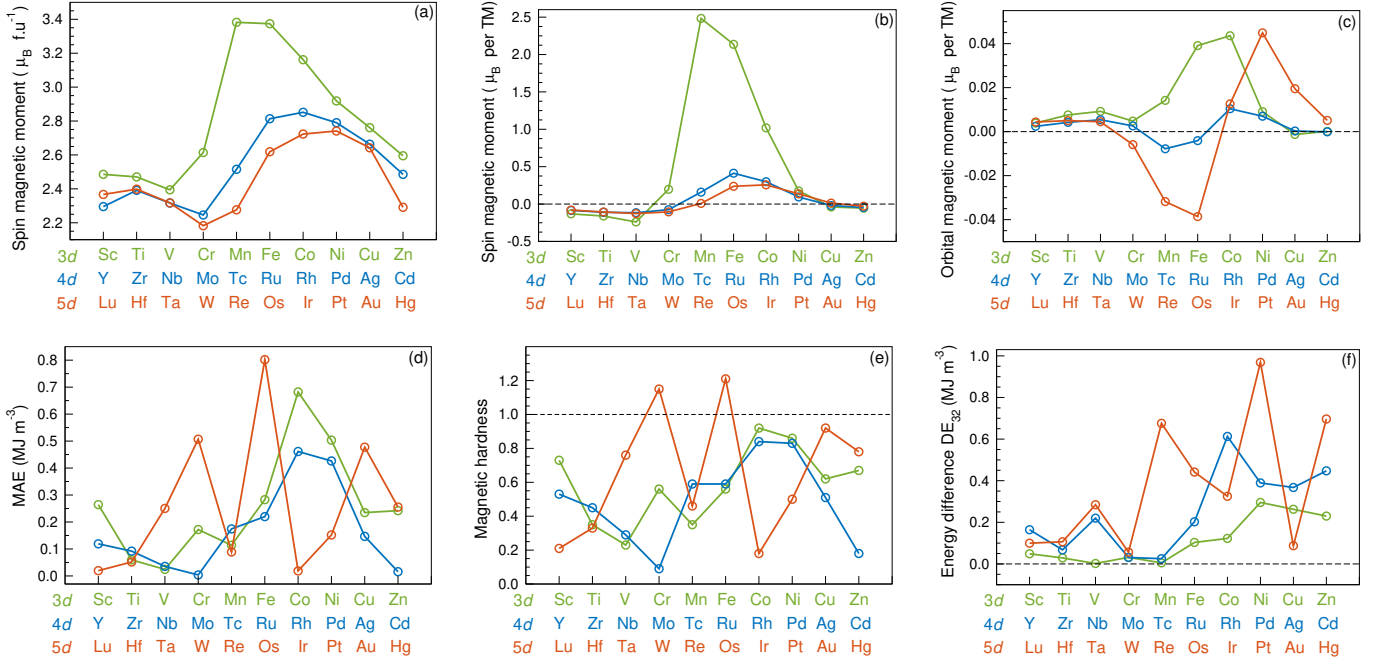


FIG. 9. The magnetic properties of ortho- Co_3C alloys with $3d$, $4d$, and $5d$ transition metals X ($\text{Co}_{11}\text{X}_1\text{C}_4$): (a) total spin magnetic moment (per formula unit of two atoms); (b, c) spin and orbital magnetic moments on substitution atoms X (per TM atom); (d) magnetocrystalline anisotropy energy (MAE); (e) magnetic hardness; and (f) energy difference (DE_{32}) between the two higher energies among the three total energies calculated along the three main crystallographic axes. The calculations were performed with FPLO18 code using the PBE functional and supercell approach.

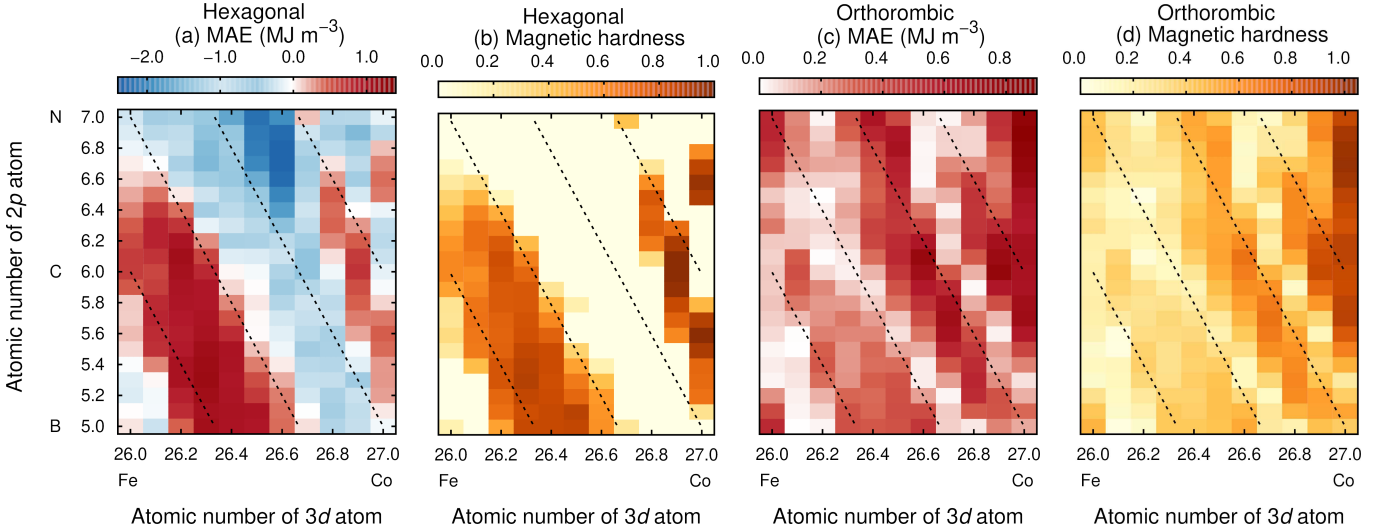


FIG. 10. (a,c) Magnetocrystalline anisotropy energy and (b,d) magnetic hardness as dependencies on the average atomic number of the elements $3d$ and $2p$ calculated for hexagonal and orthorhombic phase of $(\text{Fe},\text{Co})_3(\text{B},\text{C},\text{N})$ pseudobinary alloys. Calculations performed with virtual crystal approximation (VCA), using the FPLO18 code with PBE exchange-correlation potential. Along the dashed isolines, the total atomic number per formula (and thus the total number of electrons per formula) is constant.

alloys range from Fe_3C to Fe_3B , the magnetic moment grows by about 10% and the Curie temperature linearly increases from 481 K to the impressive 824 K [21]. A similar significant increase in Curie temperature during alloying at the p -site was also observed for the transition from Fe_5PB_2 to Fe_5SiB_2 , where an alloying element with one less atomic number was also used [89]. Medvedeva *et*

al. have shown by supercell method that B alloying increases the magnetic moment of ortho- $\text{Fe}_3(\text{B},\text{C})$ borocarbides and stabilizes them [53]. Ande and Sluiter, also using supercell calculations, tested the effect of substitution of Al, Si, P, or S at the C-site in ortho- Fe_3C on the stability of solid solutions [50]. Moreover, the hexa- Fe_3N nitride has a negative formation energy, hence it

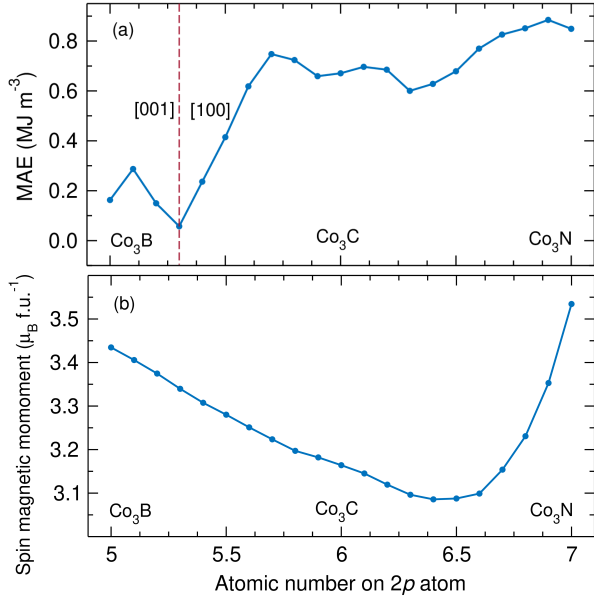


FIG. 11. Dependence of (a) magnetocrystalline anisotropy energy and (b) total spin magnetic moment on the average atomic number of elements $2p$ calculated for orthorhombic $\text{Co}_3(\text{B,C,N})$ alloys. The red dashed line separates the regions with different directions of magnetic easy axis. Calculations were performed with virtual crystal approximation (VCA), using the FPLO18 code with PBE exchange-correlation potential.

TABLE V. Magnetocrystalline anisotropy energy [MAE (MJ m^{-3})] and magnetic hardness [κ] of selected $(\text{Fe,Co})_3(\text{B,C,N})$ compositions with hexagonal and orthorhombic symmetries calculated with FPLO18 code using PBE functional and virtual crystal approximation to model alloying.

Compound/Alloy	Hexagonal		Orthorhombic	
	MAE	κ	MAE	κ
Fe_3B	0.05	0.18	0.53	0.50
Fe_3C	0.68	0.63	0.11	0.21
Fe_3N	-0.25	0	0.55	0.45
Co_3B	-0.09	0	0.16	0.41
Co_3C	-0.15	0	0.67	0.91
Co_3N	-0.15	0	0.82	0.92
$\text{Co}_3(\text{C}_{0.3}\text{N}_{0.7})$	–	–	0.83	1.02
$\text{Co}_3(\text{B}_{0.4}\text{C}_{0.6})$	0.47	1.01	–	–
$(\text{Fe}_{0.1}\text{Co}_{0.9})_3\text{C}$	0.75	1.13	–	–
$(\text{Fe}_{0.1}\text{Co}_{0.9})_3(\text{C}_{0.9}\text{N}_{0.1})$	0.69	1.10	–	–
$(\text{Fe}_{0.7}\text{Co}_{0.3})_3(\text{B}_{0.7}\text{C}_{0.3})$	1.19	0.91	–	–

stabilizes the hexagonal nitrocarbides [29]. The hexagonal $\text{Fe}_3(\text{C,N})$ powder consisting of 5% N was previously synthesized [29] and classified as magnetically soft.

In this section, we extend the study of $(\text{Fe,Co})_3\text{C}$ alloys, and analyze the alloying at both the $3d$ and $2p$ sites within a single model. We consider $(\text{Fe,Co})_3(\text{B,C,N})$ al-

loys with concentration range at $3d$ site from Fe to Co (atomic numbers from 26 to 27) and at $2p$ site from B, through C, to N (atomic numbers from 5 to 7). In Figure 10, we show maps of MAE and magnetic hardness for hexagonal and orthorhombic alloys. Furthermore, in Table V, we present calculated values of MAE and magnetic hardness for stoichiometric compounds and for alloys with the highest determined magnetic hardnesses.

Studying alloying simultaneously at $3d$ and $2p$ sites allows conclusions to be drawn about the basic nature of the MAE. Particularly noticeable in MAE maps are diagonal stripes, see Fig. 10. It means that the MAE does not depend on the details of the composition, but on the total atomic number of the system (or equivalent total number of electrons). The dependence of the MAE on the number of electrons is in agreement with the model of the origin of the MAE as a subtle property, which depends on the details of the valence band form and its filling level [78].

The hexagonal $(\text{Fe,Co})_3(\text{B,C,N})$ system exhibit MAE from -2.4 to 1.19 MJ m^{-3} , see Fig. 10. The highest value of MAE (1.19 MJ m^{-3}) is obtained for $(\text{Fe}_{0.7}\text{Co}_{0.3})_3(\text{B}_{0.7}\text{C}_{0.3})$. Several other compositions also exhibit magnetic hardness above unity, see Table V. Moreover, the orthorhombic $(\text{Fe,Co})_3(\text{B,C,N})$ system shows only positive MAE values, while the direction of the magnetic easy axis changes. For orthorhombic phases, the highest values of magnetic hardness are observed for full Co content, agreeing with the previous results for $(\text{Fe,Co})_3\text{C}$ alloys, see Fig. 4. The highest value of MAE (0.83 MJ m^{-3} ; leading to magnetic hardness of 1.02) was determined for $\text{Co}_3(\text{C}_{0.3}\text{N}_{0.7})$. However, alloying with N can further destabilize orthorhombic carbides.

As we said, the most promising MAEs are observed for orthorhombic alloys with full Co content, see Fig. 10. To take a closer look at this range, in a one-dimensional Fig. 11 we again show the dependence of MAE on element concentration at the $2p$ position, along with a plot of spin magnetic moment. At the center of B-C-N range is the ortho- Co_3C compound, known from previous discussion as a promising composition for hard magnetic applications. Although raising the nitrogen concentration leads to an increase in MAE, for reasons related to the instability of the ortho- Co_3N phase, a better approach may be to alloy ortho- Co_3C with boron, which should both stabilize the system and raise its Curie temperature. Experimental Curie temperatures of ortho- Co_3C [23] and ortho- Co_3B [16] are 650 K and 750 K, respectively. Moreover, the dependence of the magnetic moment on the concentration of $2p$ atoms is non-intuitive, see Fig. 11(b). While in the range from B to C it is qualitatively consistent with the ten percent decrease in magnetic moment measured for the isostructural $\text{Fe}_3(\text{B,C})$ phase [21], in the range from C to N the magnetic moment shows a surprising minimum. Furthermore, the calculated MAE of Co_3B of less than 0.2 MJ m^{-3} is much lower than the corresponding room-temperature experimental value of 0.65 MJ m^{-3} [16]. The discrepancy is due to, among other things, the dependence of MAE on temperature,

as the calculations were performed at 0 K.

In summary, the alloying at the $2p$ position, as discussed in this section, allows for the control of MAE, magnetic moment, and Curie temperature. Furthermore, the aforementioned observation that MAE can depend on the total number of electrons in the system can prove useful in the designing of new compositions of magnetically hard materials.

IV. SUMMARY AND CONCLUSIONS

In this study, we employed a first-principles approach to investigate the influence of composition on the magnetic properties of Fe_3C -type alloys. The objective was to identify alloys that exhibit enhanced magnetic hardness. This work has been divided into four parts. In the first, we have presented results for Fe_3C and Co_3C compounds, in the second for $(\text{Fe},\text{Co})_3\text{C}$ alloys, in the third for Fe_3C and Co_3C alloys with transition metals, and in the fourth for $(\text{Fe},\text{Co})_3(\text{B-C-N})$ alloys. In each instance, both hexagonal and orthorhombic structures were analyzed. For Fe_3C and Co_3C compounds, we examined what effect the form of the exchange-correlation potential has on the MAE and magnetic moment. By determining the dependence of the MAE on the fixed spin (magnetic) moment, we have preliminarily identified the range of MAE that the systems under consideration can adopt under varying temperatures or alloy compositions. The outcome of the investigation was not particularly encouraging. Of the four compounds considered, none proved to be magnetically hard. The highest magnetic hardness of 0.91 was predicted for ortho- Co_3C . In order to investigate the magnetic properties of $(\text{Fe},\text{Co})_3\text{C}$ alloys, we employed the virtual crystal approximation to calculate changes in magnetic properties as a function of

Co concentration. This analysis led to the identification of magnetically hard Co-rich hexa- $(\text{Fe}_{0.1}\text{Co}_{0.9})_3\text{C}$ phase. Furthermore, we considered a series of hexa- Fe_3C , ortho- Fe_3C , and ortho- Co_3C alloys with transition metals at a concentration of 1/12 on Fe or Co site. Calculations of the Curie temperature and magnetic hardness do not indicate that alloying with transition metals increases their potential for permanent magnet applications. Finally, we found that a considerable proportion of the ortho- $\text{Co}_3(\text{B-C-N})$ alloys are magnetically hard, of which boron substitution raises the Curie temperature and improves stability.

The most universal result of this work is the interpretation of the two-dimensional dependence of MAE on concentration at both $3d$ and $2p$ positions of $(\text{Fe-Co})_3(\text{B-C-N})$ alloys. The diagonal stripes visible in the MAE maps are interpreted as the dependence of MAE on the total number of electrons in the system, which is weakly responsive to the details of the occupancies at individual sites. This type of dependence offers a novel perspective on the design of compositions of hard magnetic materials.

ACKNOWLEDGMENTS

We acknowledge the financial support from the National Science Center of Poland under grants DEC-2019/35/O/ST5/02980 – PRELUDIUM BIS 1 (J.S.-A.) and DEC-2021/41/B/ST5/02894 – OPUS 21 (J.R.-G. and MW). Part of the calculation was made in the Poznan Supercomputing and Networking Centre (PSNC/PCSS). We thank P. Leśniak and D. Depcik for compiling the scientific software and managing the computer cluster at the Institute of Molecular Physics, Polish Academy of Sciences. We thank Z. Śniadecki and K. Synoradzki for reading the manuscript and providing valuable comments.

-
- [1] O. Gutfleisch, M. A. Willard, E. Brück, C. H. Chen, S. G. Sankar, and J. P. Liu, Magnetic materials and devices for the 21st century: Stronger, lighter, and more energy efficient, *Adv. Mater.* **23**, 821 (2011).
 - [2] F. Ronning and S. Bader, Rare earth replacement magnets, *J. Phys.: Condens. Matter* **26**, 060301 (2014).
 - [3] L. H. Lewis and F. Jiménez-Villacorta, Perspectives on permanent magnetic materials for energy conversion and power generation, *Metall. Mater. Trans. A* **44**, 2 (2013).
 - [4] B. J. Smith, M. E. Riddle, M. R. Earlam, C. Iloeje, and D. Diamond, *Rare Earth Permanent Magnets: Supply Chain Deep Dive Assessment*, Tech. Rep. (USDOE Office of Policy, Washington DC (United States), 2022).
 - [5] K. Bourzac, The rare-earth crisis, *Technology Review* **114**, 58 (2011).
 - [6] M. D. Kuz'min, K. P. Skokov, H. Jian, I. Radulov, and O. Gutfleisch, Towards high-performance permanent magnets without rare earths, *J. Phys. Condens. Matter* **26**, 064205 (2014).
 - [7] K. P. Skokov and O. Gutfleisch, Heavy rare earth free, free rare earth and rare earth free magnets - vision and reality, *Scr. Mater.* **154**, 289 (2018).
 - [8] J. Cui, M. Kramer, L. Zhou, F. Liu, A. Gabay, G. Hadjipanayis, B. Balasubramanian, and D. Sellmyer, Current progress and future challenges in rare-earth-free permanent magnets, *Acta Mater.* **158**, 118 (2018).
 - [9] D. Li, Y. Li, D. Pan, Z. Zhang, and C.-J. Choi, Prospect and status of iron-based rare-earth-free permanent magnetic materials, *J. Magn. Magn. Mater.* **469**, 535 (2019).
 - [10] A. Vishina, O. Y. Vekilova, T. Björkman, A. Bergman, H. C. Herper, and O. Eriksson, High-throughput and data-mining approach to predict new rare-earth free permanent magnets, *Phys. Rev. B* **101**, 094407 (2020).
 - [11] J. M. D. Coey, Perspective and Prospects for Rare Earth Permanent Magnets, *Engineering* **6**, 119 (2020).
 - [12] Y. Zhang, G. S. Chaubey, C. Rong, Y. Ding, N. Poudyal, P.-c. Tsai, Q. Zhang, and J. P. Liu, Controlled synthesis and magnetic properties of hard magnetic Co_xC ($x=2,3$) nanocrystals, *J. Magn. Magn. Mater.* **323**, 1495 (2011).
 - [13] K. J. Carroll, Z. J. Huba, S. R. Spurgeon, M. Qian, S. N. Khanna, D. M. Hudgins, M. L. Taheri, and E. E. Carpenter, Magnetic properties of Co_2C and Co_3C nanopar-

- ticles and their assemblies, *Appl. Phys. Lett.* **101**, 012409 (2012).
- [14] K. Rohith Vinod, P. Saravanan, M. Sakar, V. T. P. Vinod, M. Cernik, and S. Balakumar, Large scale synthesis and formation mechanism of highly magnetic and stable iron nitride (ϵ -Fe₃N) nanoparticles, *RSC Adv.* **5**, 56045 (2015).
- [15] A. A. El-Gendy, M. Bertino, D. Clifford, M. Qian, S. N. Khanna, and E. E. Carpenter, Experimental evidence for the formation of CoFe₂C phase with colossal magnetocrystalline-anisotropy, *Appl. Phys. Lett.* **106**, 213109 (2015).
- [16] S. Pal, K. Skokov, T. Groeb, S. Ener, and O. Gutfleisch, Properties of magnetically semi-hard (Fe_xCo_{1-x})₃B compounds, *J. Alloys Compd.* **696**, 543 (2017).
- [17] S. Wu, B. Balamurugan, X. Zhao, S. Yu, M. C. Nguyen, Y. Sun, S. Valloppilly, D. J. Sellmyer, K. Ho, and C. Wang, Exploring new phases of Fe_{3-x}Co_xC for rare-earth-free magnets, *J. Phys. D Appl. Phys.* **50**, 215005 (2017).
- [18] J. Mohapatra, M. Xing, J. Elkins, and J. P. Liu, Hard and semi-hard magnetic materials based on cobalt and cobalt alloys, *J. Alloys Compd.* **824**, 153874 (2020).
- [19] P. V. Marshall, Z. Alptekin, S. D. Thiel, D. Smith, Y. Meng, and J. P. S. Walsh, High-Pressure Synthesis of Bulk Cobalt Cementite, Co₃C, *Chem. Mater.* **33**, 9601 (2021).
- [20] H.-j. Choe, T. Terai, T. Fukuda, T. Kakeshita, S. Yamamoto, and M. Yonemura, Easy axis of magnetization of Fe₃C prepared by an electrolytic extraction method, *J. Magn. Magn. Mater.* **417**, 1 (2016).
- [21] M. E. Nicholson, Solubility of boron in Fe₃C and variation of saturation magnetization, curie temperature, and lattice parameter of Fe₃(C,B) with composition, *JOM* **9**, 1 (1957).
- [22] H. Bhadeshia, Cementite, *Int. Mater. Rev.* **65**, 1 (2020).
- [23] A. A. El-Gendy, M. Qian, Z. J. Huba, S. N. Khanna, and E. E. Carpenter, Enhanced magnetic anisotropy in cobalt-carbide nanoparticles, *Appl. Phys. Lett.* **104**, 023111 (2014).
- [24] A. A. El-Gendy, T. Almuqaiteeb, and E. E. Carpenter, Co_xC nanorod magnets: highly magnetocrystalline anisotropy with lower curie temperature for potential applications, *J. Magn. Magn. Mater.* **348**, 136 (2013).
- [25] A. Kagawa and T. Okamoto, Lattice Parameters of Cementite in Fe-C-X (X = Cr, Mn, Mo, and Ni) Alloys, *Trans. Jpn. Inst. Met.* **20**, 659 (1979).
- [26] P. Schaaf, S. Wiesen, and U. Gonser, Mössbauer study of iron carbides: Cementite (Fe, M)₃C (M = Cr, Mn) with various manganese and chromium contents, *Acta Metall. Mater.* **40**, 373 (1992).
- [27] M. Umemoto, Z. G. Liu, K. Masuyama, and K. Tsuchiya, Influence of alloy additions on production and properties of bulk cementite, *Scripta Materialia* **45**, 391 (2001).
- [28] X. Wang, P. Zhang, W. Wang, X. Lei, and H. Yang, Fe₃C and Mn doped Fe₃C nanoparticles: Synthesis, morphology and magnetic properties, *RSC Adv.* **5**, 57828 (2015).
- [29] S. A. Rounaghi, D. E. P. Vanpoucke, E. Esmaeili, S. Scudino, and J. Eckert, Synthesis, characterization and thermodynamic stability of nanostructured ϵ -iron carbonitride powder prepared by a solid-state mechanochemical route, *J. Alloys Compd.* **778**, 327 (2019).
- [30] W. Zhang, Z. Lv, Z. Shi, S. Sun, Z. Wang, and W. Fu, Electronic, magnetic and elastic properties of ϵ -phases Fe₃X (X = B, C, N) from density-functional theory calculations, *J. Magn. Magn. Mater.* **324**, 2271 (2012).
- [31] L. Hui, Z.-Q. Chen, Z. Xie, and C. Li, Stability, Magnetism and Hardness of Iron Carbides from First-Principles Calculations, *J. Supercond. Nov. Magn.* **31**, 353 (2018).
- [32] N. I. Medvedeva, I. R. Shein, M. A. Konyaeva, and A. L. Ivanovskii, Effect of chromium on the electronic structure and magnetic properties of cementite, *Phys. Metals Metallogr.* **105**, 568 (2008).
- [33] I. R. Shein, N. I. Medvedeva, and A. L. Ivanovskii, Electronic structure and magnetic properties of Fe₃C with 3d and 4d impurities, *Phys. Status Solidi B* **244**, 1971 (2007).
- [34] O. Buggenhoudt, T. Schuler, C.-C. Fu, and J.-L. Béchéde, Predicting carbon diffusion in cementite from first principles, *Phys. Rev. Mater.* **5**, 063401 (2021).
- [35] C. M. Fang, M. A. van Huis, and H. W. Zandbergen, Structural, electronic, and magnetic properties of iron carbide Fe₇C₃ phases from first-principles theory, *Phys. Rev. B* **80**, 224108 (2009).
- [36] A. Dick, F. Körmann, T. Hickel, and J. Neugebauer, Ab initio based determination of thermodynamic properties of cementite including vibronic, magnetic, and electronic excitations, *Phys. Rev. B* **84**, 125101 (2011).
- [37] I. R. Shein, N. I. Medvedeva, and A. L. Ivanovskii, Electronic and structural properties of cementite-type M₃X (M=Fe, Co, Ni; X=C or B) by first principles calculations, *Phys. B Condens. Matter* **371**, 126 (2006).
- [38] W. C. Chiou Jr and E. A. Carter, Structure and stability of Fe₃C-cementite surfaces from first principles, *Surf. Sci.* **530**, 88 (2003).
- [39] H. Faraoun, Y. Zhang, C. Esling, and H. Aourag, Crystalline, electronic, and magnetic structures of θ -Fe₃C, χ -Fe₅C₂, and η -Fe₂C from first principle calculation, *J. Appl. Phys.* **99**, 093508 (2006).
- [40] D. Odkhoo, N. Tsogbadrakh, A. Dulmaa, N. Otgonzul, and D. Naranchimeg, Substitution- and strain-induced magnetic phase transition in iron carbide, *J. Korean Phys. Soc.* **69**, 1335 (2016).
- [41] F. Chen, H. Jiang, Y. Zhang, S. Tian, Y. Yang, R. Zhang, H. Zhong, and X. Tang, First-principles calculation of bonding and hydrogen trapping mechanism of Fe₃C/ α -Fe interface, *J. Mater. Res. Technol.* **26**, 6782 (2023).
- [42] X. Wu, Q. Tian, W. Shen, X. Xu, and J. Fu, An Atomistic Structure of Cementite (M₃C, M = Fe, Cr, Mn) in Carbon Steel, *Phys. Metals Metallogr.* **124**, 1404 (2023).
- [43] X. Yuan, Y. Zhou, C. Huo, W. Guo, Y. Yang, Y. Li, and X. Wen, Crystal structure prediction approach to explore the iron carbide phases: Novel crystal structures and unexpected magnetic properties, *J. Phys. Chem. C* **124**, 17244 (2020).
- [44] Z. Lv, F. Zhang, S. Sun, Z. Wang, P. Jiang, W. Zhang, and W. Fu, First-principles study on the mechanical, electronic and magnetic properties of Fe₃C, *Comput. Mater. Sci.* **44**, 690 (2008).
- [45] M. A. Konyaeva and N. I. Medvedeva, Electronic structure, magnetic properties, and stability of the binary and ternary carbides (Fe,Cr)₃C and (Fe,Cr)₇C₃, *Phys. Solid State* **51**, 2084 (2009).
- [46] Z. Lv, W. Fu, S. Sun, X. Bai, Y. Gao, Z. Wang, and P. Jiang, First-principles study on the electronic structure, magnetic properties and phase stability of alloyed cementite with Cr or Mn, *J. Magn. Magn. Mater.* **323**, 915 (2011).

- [47] J.-p. Yang, J. Chen, W. Li, P.-d. Han, and L.-n. Guo, First-principles study on electronic structure, magnetic and dielectric properties of Cr-doped Fe_3C , *J. Cent. South Univ.* **23**, 2173 (2016).
- [48] C. Wang, Z. Lv, W. Fu, Y. Li, S. Sun, and B. Wang, Electronic properties, magnetic properties and phase stability of alloyed cementite $(\text{Fe}, \text{M})_3\text{C}$ ($\text{M} = \text{Co}, \text{Ni}$) from density-functional theory calculations, *Solid State Sci.* **13**, 1658 (2011).
- [49] Y. Gao, B. Wang, M. Guo, Z. Lv, S. Sun, R. Zhang, and W. Fu, First-principles study on surface structural, magnetic and electronic properties of alloyed cementite with Co or Ni, *Comput. Mater. Sci.* **85**, 154 (2014).
- [50] C. K. Ande and M. H. Sluiter, First-principles calculations on stabilization of iron carbides (Fe_3C , Fe_5C_2 , and $\eta\text{-Fe}_2\text{C}$) in steels by common alloying elements, *Metall. Mater. Trans. A* **43**, 4436 (2012).
- [51] V. Razumovskiy and G. Ghosh, A first-principles study of cementite (Fe_3C) and its alloyed counterparts: Structural properties, stability, and electronic structure, *Comput. Mater. Sci.* **110**, 169 (2015).
- [52] Z. Lv, W. Fu, S. Sun, Z. Wang, W. Fan, and M. Qv, Structural, electronic and magnetic properties of cementite-type Fe_3X ($\text{X} = \text{B}, \text{C}, \text{N}$) by first-principles calculations, *Solid State Sci.* **12**, 404 (2010).
- [53] N. Medvedeva, I. Shein, O. Y. Gutina, and A. Ivanovskii, Simulation of the structural, electronic, and magnetic properties of $\text{Fe}_3\text{C}_{1-x}\text{B}_x$ borocementites, *Phys. Solid State* **49**, 2298 (2007).
- [54] J. Marciniak, M. Werwiński, and J. Rychły-Gruszecka, First-principles study of the magnetic anisotropy of ultrathin B-, C-, and N-doped FeCo films, *J. Magn. Magn. Mater.* **589**, 171563 (2024).
- [55] D. Fruchart, P. Chaudouet, R. Fruchart, A. Rouault, and J. Senateur, Etudes structurales de composés de type cémentite: Effet de l'hydrogène sur Fe_3C suivi par diffraction neutronique. Spectrométrie Mössbauer sur FeCo_2B et Co_3B dopés au ^{57}Fe , *J. Solid State Chem.* **51**, 246 (1984).
- [56] H. L. Yakel, Crystal structures of stable and metastable iron-containing carbides, *Int. Met. Rev.* **30**, 17 (1985).
- [57] K. Koepnik and H. Eschrig, Full-potential nonorthogonal local-orbital minimum-basis band-structure scheme, *Phys. Rev. B* **59**, 1743 (1999).
- [58] I. Opahle, K. Koepnik, and H. Eschrig, Full-potential band-structure calculation of iron pyrite, *Phys. Rev. B* **60**, 14035 (1999).
- [59] J. P. Perdew, K. Burke, and M. Ernzerhof, Generalized Gradient Approximation Made Simple, *Phys. Rev. Lett.* **77**, 3865 (1996).
- [60] K. Momma and F. Izumi, *VESTA*: A three-dimensional visualization system for electronic and structural analysis, *J. Appl. Crystallogr.* **41**, 653 (2008).
- [61] U. Von Barth and L. Hedin, A local exchange-correlation potential for the spin polarized case. i, *J. Phys. C: Solid State Phys.* **5**, 1629 (1972).
- [62] J. P. Perdew and A. Zunger, Self-interaction correction to density-functional approximations for many-electron systems, *Phys. Rev. B* **23**, 5048 (1981).
- [63] J. P. Perdew and Y. Wang, Accurate and simple analytic representation of the electron-gas correlation energy, *Phys. Rev. B* **45**, 13244 (1992).
- [64] J. Snarski-Adamski and M. Werwiński, Searching for magnetically hard monoborides (and finding a few): A first-principles investigation, arXiv preprint [10.48550/arXiv.2403.00138](https://arxiv.org/abs/10.48550/arXiv.2403.00138) (2024).
- [65] O. V. Zhdanova, M. B. Lyakhova, and Yu. G. Pastushenkov, Magnetic properties and domain structure of FeB single crystals, *Met. Sci. Heat Treat.* **55**, 68 (2013).
- [66] B. L. Gyorffy, A. J. Pindor, J. Staunton, G. M. Stocks, and H. Winter, A first-principles theory of ferromagnetic phase transitions in metals, *J. Phys. F Met. Phys.* **15**, 1337 (1985).
- [67] J. Kudrnovský, I. Turek, V. Drchal, F. Máca, P. Weinberger, and P. Bruno, Exchange interactions in III-V and group-IV diluted magnetic semiconductors, *Phys. Rev. B* **69**, 115208 (2004).
- [68] V. Heine, J. H. Samson, and C. M. M. Nex, Theory of local magnetic moments in transition metals, *J. Phys. F Met. Phys.* **11**, 2645 (1981).
- [69] P. Soven, Coherent-potential model of substitutional disordered alloys, *Phys. Rev.* **156**, 809 (1967).
- [70] G. Miyamoto, J. Oh, K. Hono, T. Furuhashi, and T. Maki, Effect of partitioning of Mn and Si on the growth kinetics of cementite in tempered Fe-0.6 mass% C martensite, *Acta Mater.* **55**, 5027 (2007).
- [71] E. Martinez-Teran, A. K. Cordeiro, and A. A. El-Gendy, Nucleation of Co_3C Magnetic Nanoparticles Using Supercritical Condition of Ethanol, *JOM* **71**, 4940 (2019).
- [72] A.-M. Zieschang, J. D. Bocarsly, J. Schuch, C. V. Reichel, B. Kaiser, W. Jaegermann, R. Seshadri, and B. Albert, Magnetic and Electrocatalytic Properties of Nanoscale Cobalt Boride, Co_3B , *Inorg. Chem.* **58**, 16609 (2019).
- [73] R. Wu and A. J. Freeman, Spin-orbit induced magnetic phenomena in bulk metals and their surfaces and interfaces, *J. Magn. Magn. Mater.* **200**, 498 (1999).
- [74] D. Jiang and E. A. Carter, Carbon dissolution and diffusion in ferrite and austenite from first principles, *Phys. Rev. B* **67**, 214103 (2003).
- [75] S. N. Budko and M. V. Mamonova, Calculation of the exchange integrals for $\text{Co}_{1-x}\text{Ni}_x$ alloy by Korring-Kohn-Rostoker method, *J. Phys.: Conf. Ser.* **1389**, 012144 (2019).
- [76] J. Snarski-Adamski and M. Werwiński, Effect of transition metal doping on magnetic hardness of CeFe_{12} -based compounds, *J. Magn. Magn. Mater.* **554**, 169309 (2022).
- [77] T. Burkert, L. Nordström, O. Eriksson, and O. Heinonen, Giant magnetic anisotropy in tetragonal FeCo alloys, *Phys. Rev. Lett.* **93**, 027203 (2004).
- [78] A. Edström, M. Werwiński, D. Iuşan, J. Rusz, O. Eriksson, K. Skokov, I. Radulov, S. Ener, M. Kuz'Min, J. Hong, *et al.*, Magnetic properties of $(\text{Fe}_{1-x}\text{Co}_x)_2\text{B}$ alloys and the effect of doping by 5d elements, *Phys. Rev. B* **92**, 174413 (2015).
- [79] W. Marciniak and M. Werwiński, Structural and magnetic properties of Fe-Co-C alloys with tetragonal deformation: A first-principle study, *Phys. Rev. B* **108**, 214433 (2023).
- [80] C. T. Chen, Y. U. Idzerda, H.-J. Lin, N. V. Smith, G. Meigs, E. Chaban, G. H. Ho, E. Pellegrin, and F. Sette, Experimental Confirmation of the X-Ray Magnetic Circular Dichroism Sum Rules for Iron and Cobalt, *Phys. Rev. Lett.* **75**, 152 (1995).
- [81] V. A. Barinov, V. A. Tsurin, V. A. Kazantsev, and V. T. Surikov, Carbonization of $\alpha\text{-Fe}$ upon mechanical alloying, *Phys. Met. Metallogr.* **115**, 53 (2014).
- [82] G. Le Caer, J. M. Dubois, M. Pijolat, V. Perrichon, and P. Bussiere, Characterization by Moessbauer spectroscopy of iron carbides formed by Fischer-Tropsch synthesis, *J. Phys. Chem.* **86**, 4799 (1982).

- [83] V. G. Harris, Y. Chen, A. Yang, S. Yoon, Z. Chen, A. L. Geiler, J. Gao, C. N. Chinnasamy, L. H. Lewis, C. Vittoria, E. E. Carpenter, K. J. Carroll, R. Goswami, M. A. Willard, L. Kurihara, M. Gjoka, and O. Kalogirou, High coercivity cobalt carbide nanoparticles processed via polyol reaction: A new permanent magnet material, *J. Phys. Appl. Phys.* **43**, 165003 (2010).
- [84] Z. Turgut, M. S. Lucas, S. Leontsev, S. L. Semiatin, and J. Horwath, Metastable Co_3C nanocrystalline powder produced via reactive ball milling: Synthesis and magnetic properties, *J. Alloys Compd.* **676**, 187 (2016).
- [85] H. Akai, Nuclear spin-lattice relaxation of impurities in ferromagnetic iron, *Hyperfine Interact.* **43**, 253 (1988).
- [86] P. H. Dederichs, R. Zeller, H. Akai, and H. Ebert, Ab-initio calculations of the electronic structure of impurities and alloys of ferromagnetic transition metals, *J. Magn. Magn. Mater.* **100**, 241 (1991).
- [87] J. Snarski-Adamski, J. Rychły, and M. Werwiński, Magnetic properties of 3d, 4d, and 5d transition-metal atomic monolayers in Fe/TM/Fe sandwiches: Systematic first-principles study, *J. Magn. Magn. Mater.* **546**, 168828 (2022).
- [88] H. Du, A reevaluation of the Fe-N and Fe-C-N systems, *JPE* **14**, 682 (1993).
- [89] D. Hedlund, J. Cedervall, A. Edström, M. Werwiński, S. Kontos, O. Eriksson, J. Ruzs, P. Svedlindh, M. Sahlberg, and K. Gunnarsson, Magnetic properties of the Fe_5SiB_2 - Fe_5PB_2 system, *Phys. Rev. B* **96**, 094433 (2017).